



# Assessment of natural and anthropogenic aerosol air pollution in the Middle East using MERRA-2, CAMS data assimilation products, and high-resolution WRF-Chem model simulations

Alexander Ukhov<sup>1</sup>, Suleiman Mostamandi<sup>1</sup>, Arlindo da Silva<sup>2</sup>, Johannes Flemming<sup>3</sup>, Yasser Alshehri<sup>1</sup>, Illia Shevchenko<sup>1</sup>, and Georgiy Stenchikov<sup>1</sup>

<sup>1</sup>King Abdullah University of Science and Technology, Thuwal, Saudi Arabia

<sup>2</sup>NASA Goddard Space Flight Center, Green-belt, MD, USA

<sup>3</sup>European Centre for Medium-Range Weather Forecasts, Reading, UK

**Correspondence:** Georgiy Stenchikov (georgiy.stenchikov@kaust.edu.sa)

**Abstract.** Modern-Era Retrospective analysis for Research and Applications v.2 (MERRA-2), Copernicus Atmosphere Monitoring Service Operational Analysis (CAMS-OA) data assimilation products, and a regional Weather Research and Forecasting model (10 km resolution) coupled with Chemistry (WRF-Chem) were used to evaluate natural and anthropogenic aerosol air pollution in the ME during 2015-2016. Satellite and ground-based AOD observations, as well as *in situ* Particulate Matter (PM)

5 measurements for 2016, were used for validation.

WRF-Chem code was modified to correct the calculation of dust gravitational settling and aerosol optical properties. The dust emission in WRF-Chem is calibrated to fit Aerosol Optical Depth (AOD) and aerosol volume size distributions obtained from Aerosol Robotic Network (AERONET) observations. MERRA-2 was used to construct WRF-Chem initial and boundary conditions both for meteorology and chemical/aerosol species.  $SO_2$  emissions in WRF-Chem are based on the novel NASA

10  $SO_2$  emission dataset that reveals unaccounted sources over the ME.

Although aerosol fields in WRF-Chem and assimilation products are quite consistent, WRF-Chem, due to its higher spatial resolution and better  $SO_2$  emissions, is preferable for analysis of regional air-quality over the ME. The WRF-Chem's PM background concentrations exceed the World Health Organization (WHO) guidelines over the entire ME. The major contributor to PM ( $\approx 75$ – $95\%$ ) is mineral dust. In the ME urban centers and near oil recovery fields, non-dust aerosols (primarily sulfate)

15 contribute up to 26% into PM<sub>2.5</sub>. The contribution of sea salt into PM can rich up to 5%. The contribution of organic matter into PM prevails over black carbon.

## 1 Introduction

PM is a complex mixture of sea salt, sulfate, black carbon, organic matter, and mineral dust, suspended in the air. The dramatic increase in the level of air pollution in developing countries over the last decades is forced by rapid economic and population

20 growth, burning of fossil fuels, construction, and agricultural activities (Janssens-Maenhout et al., 2015). However, the primary cause of air pollution in the ME is mineral dust, and it is on the rise (Klingmüller et al., 2016). Along with Asia and Africa,



the ME significantly contributes to global dust emissions, which are in the range of 1000-2000 Tg/year (Zender et al., 2004). According to Prospero et al. (2002), the Middle East and North Africa (MENA) regions account for about half of global dust emissions. By integrating surface emissions in MERRA-2 reanalysis we found that, the total global dust emission averaged over the 2015-2016 period is about 1600 Tg/year, right in the middle of the Zender et al. (2004) estimate. The dust emission from our domain (see Fig. 1) that covers the ME and nearby areas is about 500 Tg/year, contributing  $\approx 30\%$  to the global dust mass budget. Also, frequent inflows of pollutants from Europe, Africa, and India, worsen the air quality over the Arabian Peninsula (Jish Prakash et al., 2015; Kalenderski et al., 2013; Notaro et al., 2013; Reid et al., 2008; Mohalifi et al., 1998; Kalenderski and Stenchikov, 2016; Parajuli et al., 2019). Because of the large amount of dust, the ME is one of the most polluted areas in the world. Located in the center of the northern subtropical dust belt, the Arabian Desert is the third-largest (after the Sahara and the East Asian deserts) region of dust generation, where dust plays a significant role in controlling regional climate (Cahill et al., 2017; Banks et al., 2017; Jish Prakash et al., 2016; Farahat, 2016; Kalenderski and Stenchikov, 2016; Munir et al., 2013; Alghamdi et al., 2015; Lihavainen et al., 2016; Anisimov et al., 2017; Osipov and Stenchikov, 2018).

In addition to natural dust aerosols, the ME receives high concentrations of anthropogenic PM (Karagulian et al., 2015; Al-Taani et al., 2019). The most essential anthropogenic aerosol in ME is sulfate with  $SO_2$  as a precursor, the contributions of other types of aerosols in PM, sea salt, organic matter, and black carbon are of lesser importance in the ME (Randles et al., 2017).  $SO_2$  produced in the course of power generation, water desalination, and oil recovery operations is converted photochemically into sulfate aerosol, which contributes to PM and has significant adverse effects on human health (Lelieveld et al., 2015). Sulfate aerosol concentration strongly depends upon the strength of the  $SO_2$  sources, and is subject to diurnal variability due to the photochemical reactions, and thus exhibits substantial temporal and spatial heterogeneity. Along with air-pollution, aerosols (natural and anthropogenic) alter the Earth's radiative balance and generally cool the climate playing an essential role in regional and global climate changes (Carlson and Benjamin, 1980; Miller and Tegen, 1998; Bangalath and Stenchikov, 2016; Charlson et al., 1992; Chuang et al., 1997; Myhre et al., 2013; Ramanathan et al., 2005). This aerosol direct climate effect is associated with the total content of aerosols in the atmospheric column.

The impact of aerosols on air-quality is characterized by near-surface concentrations of PM, which comprise both  $PM_{10}$  and  $PM_{2.5}$  (particles with diameters less than 10  $\mu m$  and 2.5  $\mu m$  correspondingly). Extended exposure to PM may cause cardiovascular and respiratory disease, lung cancer, and cause premature mortality on a global scale (Lelieveld et al., 2015). According to the WHO, outdoor air pollution caused 4.2 million premature deaths worldwide in 2016 (WHO, 2018). To protect human health and the environment WHO (WHO, 2006), and the National Agencies, e.g., the United States Environmental Protection Agency (US-EPA) (USEPA, 2010), European Commission (EC) (EUEA, 2008), and Kingdom Saudi Arabia Presidency of Meteorology and Environment (KSA-PME) (PME, 2012) issued the air quality regulations for PM that are presented in Table 1. The WHO regulations are the strictest, while KSA-PME regulations are the softest.

Satellite observations provide information on global aerosol abundance and spatial-temporal variability. This enables a better understanding of the sources of aerosols and associated physical processes. Passive satellite aerosol sensors like Moderate Resolution Imaging Spectrometer (MODIS), Multiangle Imaging SpectroRadiometer (MISR), Advanced Very High-Resolution Radiometer (AVHRR) are designed to measure column integrated aerosol properties. Active instruments such as Cloud-Aerosol





**Table 1.** Air quality regulations for PM<sub>2.5</sub> and PM<sub>10</sub> prescribed by WHO, US-EPA, EC, and KSA-PME, µg/m<sup>3</sup>.

	Aver. period	WHO	US-EPA	EC	KSA-PME
PM <sub>2.5</sub>	24 hours	25	35 <sup>1</sup>	-	35
	1 year	10	15 <sup>2</sup>	25	15
PM <sub>10</sub>	24 hours	50	150 <sup>4</sup>	50 <sup>3</sup>	340
	1 year	20	-	40	80

<sup>1</sup> 98th percentile, averaged over 3 years

<sup>2</sup> annual mean, averaged over 3 years

<sup>3</sup> 35 permitted exceedences per year

<sup>4</sup> not to be exceeded more than once per year on average over 3 years

Lidar with Orthogonal Polarization (CALIOPE) can, in principle, provide information on the vertical structure of aerosols, although the current generation of spaceborne lidars do not possess the necessary vertical or spectral resolution to properly characterize near surface aerosol properties. The near-surface PM concentration can not be observed from the space but is measured *in situ*. These measurements could be conducted only in a limited number of locations. For example, in Tawabini et al. (2017) the measurements of PM<sub>10</sub> concentration conducted for 21 days at Dhahran, Khobar, and Dammam (cities on the west coast of Saudi Arabia) in October-December of 2015 have shown average PM<sub>10</sub> concentrations of 177, 380, and 126 µg/m<sup>3</sup> respectively, which are higher than WHO, US-EPA, and even KSA-PME limits. The PM<sub>2.5</sub> observations in the United Arab Emirates conducted for the period 1980-2016 showed that annual mean PM<sub>2.5</sub> concentrations varied from 49 to 77 µg/m<sup>3</sup> with an overall average of 61.25 µg/m<sup>3</sup> exceeding the US-EPA standards (Al-Taani et al., 2019), and over the last 14 years PM<sub>2.5</sub> concentrations showed a positive trend. In Karagulian et al. (2019), the WRF-Chem v3.8.1 was used to simulate a dust storm over the UAE on 2 April 2015. The simulated PM<sub>10</sub> concentration peaked at 1500 µg/m<sup>3</sup>. During another severe dust storm that occurred on 18 - 22 March 2012, the AOD reached 4.5 at KAUST Campus AERONET station (Jish Prakash et al., 2015). This dust storm covered a huge area, including Iraq, Iran, Kuwait, Syria, Jordan, Israel, Lebanon, UAE, Qatar, Bahrain, Saudi Arabia, Oman, Yemen, Sudan, Egypt, Afghanistan, and Pakistan. Dust source regions along the western coast of the Arabian Peninsula were also activated. The dust emission rate calculated in WRF-Chem exceeded 500 µg m<sup>-2</sup>s<sup>-1</sup> (Jish Prakash et al., 2015). Nayebare et al. (2016); Khodeir et al. (2012); Al-Jeelani (2009); Munir et al. (2013) conducted chemical characterization of airborne PM and the general state of air pollution in Saudi Arabia's cities.

Along with observations, modern data assimilation products provide valuable information about AOD and near-surface PM concentration even in areas where satellite sensors are unreliable due to factors such as the high reflectivity of land surfaces (Shi et al., 2011). Here we evaluate two data assimilation products that assimilate atmospheric constituents: MERRA-2 (Randles et al., 2017; Buchard et al., 2017) from National Aeronautics and Space Administration (NASA) Goddard Space Flight Center (GSFC) and CAMS-OA (Flemming et al., 2015; Inness et al., 2015) from European Centre for Medium-range Weather Forecast (ECMWF). The accuracy of these data assimilation products in terms of AOD and PM concentrations was evaluated at different regions of the world (Provençal et al., 2017; Buchard et al., 2017; Cesnulyte et al., 2014; Cuevas et al., 2014). E.g., Provençal et al. (2017) tested PM surface concentrations from the MERRA Aerosol Reanalysis (predecessor of MERRA-2) against

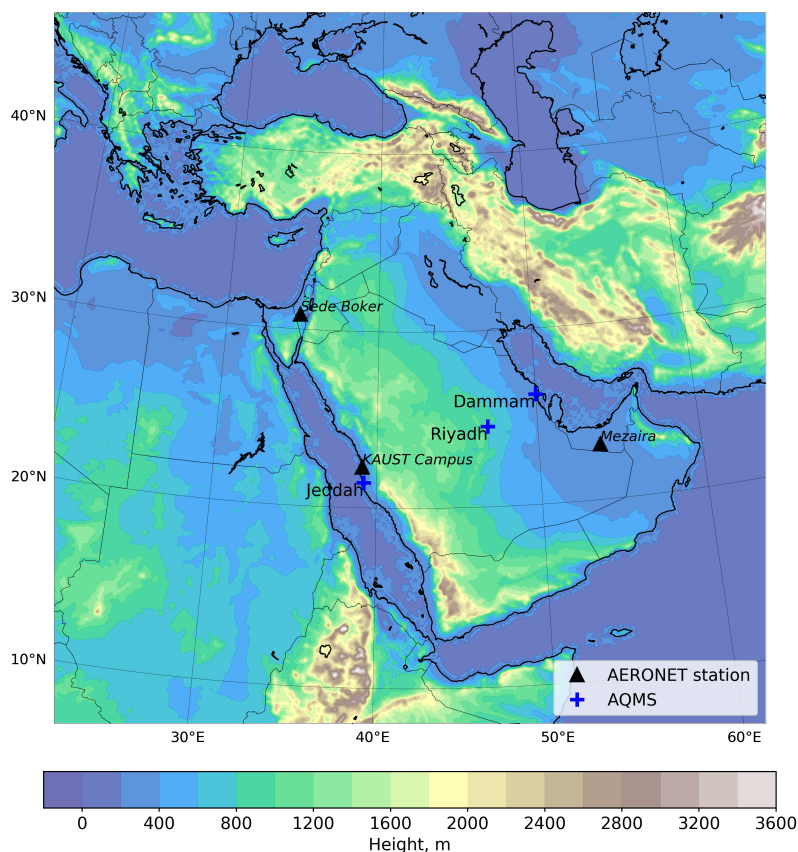


**Figure 1.** Simulation domain with marked locations of the AQMS and AERONET sites.

observations over Europe. Buchard et al. (2017) evaluated MERRA-2 surface  $PM_{2.5}$  on the global scale and over the continental United States. Excessive validation of the Monitoring Atmospheric Composition and Climate (MACC) reanalysis (predecessor of CAMS) has been conducted in Cesnulyte et al. (2014), where the model AOD is compared with the AERONET observations.

85 In Cuevas et al. (2014), atmospheric mineral dust from the MACC reanalysis has been evaluated over the MENA region for 2007–2008 using satellite and ground-based observations. MERRA-2 and CAMS-OA are global and have a relatively low spatial resolution (in comparison with the regional models), which diminishes their ability to resolve fine-scale regional spatial features. They improve the aerosol total column loadings through the assimilation of observed AOD but are not capable of assimilating the aerosol vertical structure and chemical composition. Like any other model, MERRA-2 and CAMS-OA use

90 emission inventories of anthropogenic pollutants that may be outdated and incomplete, especially in the rapidly developing parts of the world, like the ME region (McLinden et al., 2016). Here we improve the latest inventories of anthropogenic emissions in WRF-Chem using the novel  $SO_2$  emissions data set (Liu et al., 2018).



Thus in this study, we test aerosol outputs from MERRA-2, CAMS-OA, and WRF-Chem over the ME, against satellite, ground-based AOD observations, and *in situ* PM<sub>2.5</sub> and PM<sub>10</sub> measurements, and evaluate air-quality over the ME focusing on the following science questions:

1. How accurately do WRF-Chem, MERRA-2, and CAMS-OA capture the abundance of dust aerosol, its volume size, and spatial distributions over the ME, in comparison with AERONET and satellite observations?
2. How accurately do WRF-Chem, MERRA-2, and CAMS-OA capture PM surface concentrations compared with *in situ* measurements?
3. What are the contributions of dust, sea salt, sulfate, black carbon, and organic matter in PM surface concentrations?
4. What is the overall impact of PM pollution on air quality over the ME region and in the most significant ME urban centers?

The paper is organized as follows: Section 2 describes the observational datasets used in this study. Section 3 briefly describes data assimilation products. In Section 4, the WRF-Chem model setup is described. In Section 5, a comparison of the capabilities of WRF-Chem, MERRA-2, and CAMS-OA to simulate dust aerosol abundance over the ME is presented. PM pollution maps and PM levels in major urban centers of the ME obtained from the WRF-Chem simulation are also discussed. Conclusions are presented in Section 6.

## 2 Observational datasets

To evaluate the data assimilation products and WRF-Chem output, we use MODIS AOD retrievals, ground-based Aerosol Robotic Network (AERONET) AOD observations, and aerosol volume size distribution retrievals, as well as *in situ* measurements of PM surface concentrations.

### 2.1 AERONET

AERONET comprises more than 1000 CIMEL and PREDE robotic sunphotometers (made in France and Japan, respectively) which measure direct sun and sky radiances at eight wavelengths (340, 380, 440, 500, 670, 870, 940, and 1020 nm) every 15 minutes during daylight time (Holben et al., 1998). In 2012 we established the *KAUST Campus* site, which is currently the only operational AERONET site in Saudi Arabia. For this study we have chosen three AERONET sites (*KAUST Campus*, *Mezaira*, and *Sede Boker*, see Fig. 1) that routinely collected data in 2015-2016 and are located within our domain. We primarily utilized level 2.0 (cloud screened and quality assured) AERONET AOD data but used level 1.5 (cloud screened) data when level 2.0 data were not available. To facilitate comparison with the model output the 550 nm AOD is calculated using Angstrom exponent according to the following relation:

$$\frac{\tau_{\lambda}}{\tau_{\lambda_0}} = \left( \frac{\lambda}{\lambda_0} \right)^{-\alpha} \quad (1)$$



where  $\alpha$  is the Angstrom exponent,  $\tau_\lambda$  is the optical thickness at wavelength  $\lambda$ , and  $\tau_{\lambda_0}$  is the optical thickness at the reference wavelength  $\lambda_0$ . From here forward, we will presume that AOD is given or calculated at 550 nm.

In addition to direct observations of AOD, the AERONET retrieval algorithm provides column integrated Aerosol Volume  
 125 Size Distribution (AVSD)  $dV/d\ln r$  ( $\mu\text{m}^3/\mu\text{m}^2$ ) on 22 logarithmically equidistant discrete points in the range of radii between  
 0.05 and 15  $\mu\text{m}$  (Dubovik and King, 2000). We use these retrievals to evaluate the AVSDs produced by WRF-Chem, CAMS-  
 OA, and MERRA-2.

## 2.2 MODIS

MODIS instruments onboard the NASA Terra and Aqua satellites provide aerosol properties over both land and ocean with  
 130 near-daily global coverage. The high surface albedo over the desert surfaces complicates the AOD retrievals (Shi et al., 2011).  
 The standard MODIS AOD aerosol product combines two retrieval algorithms: 1) the MODIS dark-target (DT) algorithm  
 (Kaufman et al., 1997) is used over the ocean and dark areas with sufficient vegetation, 2) the Deep Blue (DB) algorithm is  
 used over bright desert surfaces of the Sahara and the ME. The uncertainties of AOD obtained with the DB algorithm are  
 $\approx 25\text{--}30\%$  (Hsu et al., 2006). From this combined product (MODIS-DB&DT v6.1) we use AOD at 550 nm level 3 data from  
 135 the daily dataset at  $1^\circ \times 1^\circ$  spatial resolution, downloaded from <https://giovanni.gsfc.nasa.gov> (Acker and Leptoukh, 2007).

Recently, a new MODIS AOD product became available that was obtained using the Multi-Angle Implementation of Atmo-  
 spheric Correction (MAIAC) algorithm (Lyapustin et al., 2018). This algorithm uses time series analysis and image processing  
 to derive the surface bidirectional reflectance function at fine spatial resolution. MAIAC uses empirically tuned, spatially vary-  
 ing, aerosol properties derived from the AERONET climatology, and provides AOD at 550 nm with 1 km spatial resolution  
 140 over land globally. We include the new MAIAC product (version 6, level 2) in the comparison between simulated and retrieved  
 AODs.

## 2.3 Surface *in situ* PM observations

To test the model-produced PM concentrations, we use observations conducted by the air quality monitoring stations (AQMS)  
 that measure surface concentrations of  $\text{PM}_{2.5}$  and  $\text{PM}_{10}$  in Riyadh, Jeddah, and Dammam (megacities of Saudi Arabia), see Fig.  
 145 1. Observations are available starting from 2016. The measurements were conducted by the Saudi Authority for Industrial Cities  
 and Technology Zones (MODON). MODON uses MP101M analyzer to continuously detect  $\text{PM}_{2.5}$  and  $\text{PM}_{10}$  concentrations  
 by measuring the absorption of low-energy  $\beta$ -radiation that is proportional to the mass of aerosol particles independently of  
 their physicochemical nature (measurement Method ISO 10473). The system satisfies the European Standards EN 12341 and  
 US EPA (40CFR part 53) for  $\text{PM}_{10}$  and EN 14907 for  $\text{PM}_{2.5}$  continuous monitoring. The PM measurements are conducted  
 150 every 15 minutes, and collected data are transmitted in real-time to servers at MODON for processing and storage. To provide  
 confidence in the operational status of the each AQMS, a comprehensive physical audit is conducted by Ricardo-AEA Ltd,  
 (<https://www.ctc-n.org/network/network-members/ricardo-aea-ltd>) quarterly.



### 3 Data assimilation products

MERRA-2 and CAMS-OA assimilate satellite and ground-based observations to provide aerosol abundance and air-quality data globally. In contrast, WRF-Chem is a free-running model and does not assimilate observations. Here, we specifically evaluate these products against observations over the ME, and compare them with the WRF-Chem output.

#### 3.1 MERRA-2

MERRA-2 (<https://gmao.gsfc.nasa.gov/reanalysis/MERRA-2>) provides meteorological and atmospheric composition fields on  $0.625^{\circ} \times 0.5^{\circ}$  latitude-longitude grid and 72 terrain-following hybrid  $\sigma - p$  model layers (Randles et al., 2017; Buchard et al., 2017). The pressure at the model top equals 0.01 hPa. MERRA-2 uses the Goddard Earth Observing System, version 5 (GEOS-5) atmospheric model (Rienecker et al., 2008), which is interactively coupled to the Goddard Global Ozone Chemistry Aerosol Radiation and Transport (GOCART) model (Chin et al., 2002) (i.e., it takes into account the effects of aerosols on radiation and model dynamics). This model simulates dust and sea salt in five size bins (see Tab. 2),  $SO_2$ , sulfate, organic and black carbon (hydrophobic and hydrophilic),  $O_3$ ,  $CO$ , dimethyl sulfide  $DMS$ , and methane sulfonic acid ( $MSA$ ). The dust density is 2600 kg/m<sup>3</sup> for all sizes. Dust and sea salt emissions are calculated in the model, depending on the near-surface wind. The dust source function is taken from Ginoux et al. (2001). For anthropogenic emissions, MERRA-2 employs the EDGAR-4.2 (Janssens-Maenhout et al., 2013) emission inventory available on a  $0.1^{\circ} \times 0.1^{\circ}$  grid. MERRA-2 assimilates AOD at 550 nm from the AVHRR (Heidinger et al., 2014) over the oceans, AOD retrievals from the MISR over bright surfaces (Kahn et al., 2005), as well as specially processed MODIS observations (but not the standard MODIS-DB&DT aerosol product) and AERONET to constrain the atmospheric aerosols.

#### 3.2 CAMS-OA

CAMS-OA (<https://atmosphere.copernicus.eu/>) has been conducted in almost real-time since July 2012. The CAMS-OA product has a resolution of  $0.8^{\circ} \times 0.8^{\circ}$  before 21 June 2016, and  $0.4^{\circ} \times 0.4^{\circ}$  after that, with 60 vertical levels. It employs the ECMWF aerosol data assimilation system developed within the Integrated Forecast System (IFS) (Morcrette et al., 2009; Benedetti et al., 2009). The extended version of the Carbon Bond chemical mechanism 5 (CB05) (Yarwood et al., 2005) is implemented in the IFS (Flemming et al., 2015). CB05 describes tropospheric chemistry with 54 species and 126 reactions. The chemistry scheme is coupled with the aerosol module.

CAMS-OA simulates five aerosol species: dust, sea salt, sulfate, organic carbon, and black carbon. To simulate dust and sea salt, it uses three dustbins (see Tab. 2). The dust density is 2600 kg/m<sup>3</sup> for all bins. Emissions of mineral dust and sea salt depend on simulated near-surface wind speed. Dust emission is parameterized following Marticorena and Bergametti (1995) with the source function adopted from Ginoux et al. (2001).  $SO_2$  oxidation into sulfate aerosol is parameterized using a prescribed latitude-dependent e-folding timescale ranging from 3 days at the equator to 8 days at the poles. The anthropogenic emissions for the chemical species are taken from the MACCity inventory (Granier et al., 2011), which is available on a  $0.5^{\circ} \times 0.5^{\circ}$  grid and covers the period 1960–2010. CAMS-OA assimilates MODIS observations.



**Table 2.** Radii ranges ( $\mu\text{m}$ ) of dust and sea salt bins used in GOCART model (WRF-Chem, MERRA-2) and in CAMS-OA.

	Bin				
	1	2	3	4	5
CAMS-OA dust	0.03-0.55	0.55-0.9	0.9-20.0	-	-
CAMS-OA sea salt	0.03-0.5	0.5-5.0	5.0-20.0	-	-
GOCART dust	0.1-1.0	1.0-1.8	1.8-3.0	3.0-6.0	6.0-10.0
GOCART sea salt	0.03-0.1	0.1-0.5	0.5-1.5	1.5-5.0	5.0-10.0

## 185 4 WRF-Chem

To calculate fine-resolution PM and sulfate fields, we use the Weather Research and Forecasting (WRF) model (Skamarock et al., 2005) coupled with chemistry (WRF-Chem v3.7.1) (Grell et al., 2005). The WRF-Chem is used for prediction and simulation of weather, air quality, and dust storms, accounting for the aerosol effect on radiation. WRF-Chem can be configured with one of the few gas-phase chemical mechanisms, photolysis, and aerosols parameterization models. WRF-Chem has been widely used for air quality simulations in different parts of the globe: East Asia (Wang et al., 2010), US (Kim et al., 2006; Chuang et al., 2011), Europe (Forkel et al., 2012; Ritter et al., 2013), South America (Archer-Nicholls et al., 2015) and Middle East (Parajuli et al., 2019).

To reduce the clock-time of our two-year calculations, we simulated each month of the 2015-2016 period separately. Each simulation starts from the last week of the previous month. This time is considered a spin-up and is excluded from post-processing. The simulation domain, shown in Fig. 1, is centered at  $28^\circ\text{N}$ ,  $42^\circ\text{E}$ , and a  $10\text{ km} \times 10\text{ km}$  horizontal grid ( $450 \times 450$  grid nodes) is employed. The vertical grid comprises 50 vertical levels with enhanced resolution closer to the ground comprising 11 model levels within the near-surface 1-km layer. The model top boundary is set at 50 hPa.

To improve the representation of the meteorological fields, we apply spectral nudging (Miguez-Macho et al., 2004) above the planetary boundary layer (PBL) ( $>5.0\text{ km}$ ) to horizontal wind components ( $U$  and  $V$ ) toward the MERRA-2 wind field. The nudging coefficient for  $U$  and  $V$  is set to be  $0.0001\text{ s}^{-1}$ . We nudge modes with wavelengths larger than 450 km. This allows us to keep the large-scale motions close to reanalysis, and leave the resolved small-scale, high-frequency features unaffected.

The aerosol/chemistry initial conditions and boundary conditions (IC&BC) are calculated using MERRA-2 output by means of the newly developed *Merra2BC* interpolation utility (see Appendix A1). To be consistent with aerosol/chemistry IC&BC, we also define the meteorological IC&BC using MERRA-2 output (see Appendix A1).

The following set of physical parameterizations was used in WRF-Chem runs. The Unified Noah land surface model (*sf\_surface\_physics*=2) and the Revised MM5 Monin-Obukhov scheme (*sf\_sfclay\_physics*=1) are chosen to represent land surface processes and surface layer physics. The Yonsei University scheme is chosen for PBL parameterization (*bl\_pbl\_physics*=1). The WRF single moment microphysics scheme (*mp\_physics*=4) is used for the treatment of cloud microphysics. The New Grell scheme (*cu\_physics*=5) is used for cumulus parameterization. The Rapid Radiative Transfer Model (RRTMG) for both short-wave (*ra\_sw\_physics*=4) and long-wave (*ra\_lw\_physics*=4) radiation is used for radiative transfer calculations. Only





the aerosol direct radiative effect is accounted for. More details on the physical parameterizations used can be found at [http://www2.mmm.ucar.edu/wrf/users/phys\\_references.html](http://www2.mmm.ucar.edu/wrf/users/phys_references.html).

#### 4.1 Gas-phase chemistry and aerosols

To calculate the atmospheric chemistry within WRF-Chem, we employ the Regional Atmospheric Chemistry Mechanism (RACM, *chem\_opt*=301) (Stockwell et al., 1997) containing 77 species and 237 reactions, which include 23 photolysis reactions. It is embedded into WRF-Chem using the Kinetic PreProcessor (KPP) (Damian et al., 2002). The role of KPP is to integrate the system of stiff nonlinear ordinary differential equations, which represents the specified set of chemical reactions. The photolysis rates are calculated on-line according to Madronich (1987) (*phot\_opt*=1). Similar to MERRA-2, the GOCART chemistry module is used to calculate  $SO_2$  to sulfate oxidation (Chin et al., 2002) by the hydroxide radical  $OH$  whose abundance is interactively simulated by RACM.

Here we use the novel OMI-HTAP  $SO_2$  emission dataset (Liu et al., 2018) based on the combination of distributed  $SO_2$  emissions from residential and transportation sectors, taken from the HTAP-2.2 inventory (Janssens-Maenhout et al., 2015) with the catalogue of the strong ( $>30$  kt/year)  $SO_2$  point emissions (Fioletov et al., 2016) built using satellite observations by Ozone Monitoring Instrument (OMI) (Levelt et al., 2006; Li et al., 2013). The catalogue contains more than 500 point sources of industrial origin, some of which are not present in the widely used EDGAR-4.2 and HTAP-2.2 emission datasets. For example, 14 previously unaccounted  $SO_2$  point emissions located in the ME (mostly in the Arabian Gulf) were detected, most of them are related to oil and gas industry. OMI-HTAP divides  $SO_2$  emissions into surface and elevated ones. We distribute the surface  $SO_2$  emissions with a constant mixing ratio in the 0-1000 m layer, and elevated emissions in 120-1000 m layer. All other constituents (PM, black and organic carbon, etc.), including  $SO_2$  shipping emissions, are taken from the HTAP-2.2 inventory and are treated as surface emissions.

To calculate aerosols we employ the GOCART (Chin et al., 2002) aerosol model (*chem\_opt*=301). It is the same microphysical model as that used in MERRA-2 (see Sec. 3.1). Dust and sea salt size distributions in WRF-Chem are approximated by the same five dust and sea-salt size bins as those in MERRA-2 (Tab. 2). However, only the last four "salt" bins in Tab. 2 are used in WRF-Chem, as the first bin appears to be very poorly populated. Dust density is assumed to be  $2500 \text{ kg/m}^3$  for the first dustbin and  $2650 \text{ kg/m}^3$  for 2-5 dustbins. Emission of sea salt is calculated according to Gong (2003). Dust emission from the surface is calculated using the GOCART emission scheme (Ginoux et al., 2001) (*dust\_opt*=1). Dust emission mass flux,  $F_p$  ( $\mu\text{g m}^{-2} \text{ s}^{-1}$ ) in each dustbin  $p=1,2,\dots,5$  is defined by the relation:

$$F_p = \begin{cases} CS_s u_{10m}^2 (u_{10m} - u_t), & \text{if } u_{10m} > u_t \\ 0, & \text{otherwise} \end{cases} \quad (2)$$

where,  $C$  has the dimension of ( $\mu\text{g s}^2 \text{ m}^{-5}$ ) and is a spatially uniform factor which controls the magnitude of dust emission flux;  $S$  is the spatially nonuniform topographic source function (Ginoux et al., 2001) that characterizes the spatial distribution



240 of dust emissions;  $u_{10m}$  is the horizontal wind speed at 10 m;  $u_t$  is the threshold velocity, which depends on particle size and surface wetness;  $s_p$  is a fraction of mass emitted into dustbin  $p$ ,  $\sum s_p = 1$ .

To avoid natural dust emission in urban areas, we use the built-in WRF-Chem the U.S. Geological Survey (USGS) 24-category land-use data set (Anderson, 1976). We modify the source function  $S$  using the following expression:

$$S = (1.0 - \text{URBAN\_MASK}) \cdot S \quad (3)$$

245 where  $\text{URBAN\_MASK}$  is the USGS “Urban and Built-up Land” mask field. It has the sense of a fraction of urban area in a grid-cell and ranges from 0 to 1. Grid cells with  $\text{URBAN\_MASK}=1$  do not produce natural dust emissions. We do not account for anthropogenic dust emissions within cities, and therefore potentially underestimate urban dust pollution.

As in our previous studies (Kalenderski et al., 2013; Jish Prakash et al., 2015; Anisimov et al., 2017), we tune dust emissions to fit the daily average AOD from the AERONET stations located within the domain. For this purpose, the parameter  $C$  from  
 250 Eq. (2) has been adjusted to achieve the best agreement between simulated and observed AOD at *KAUST Campus*, *Mezaira*, and *Sede Boker* AERONET sites, see Fig. 1. Both simulations and observations represent the total AOD with contributions from all types of aerosols. Because dust dominates all other aerosols in the ME, we choose to tune only the dust emissions.

Obtained during test runs,  $C$  value of 0.5 is kept constant in all subsequent production runs. We also tune  $s_p$  from Eq. (2) to better reproduce the AVSDs provided by AERONET inversion algorithm. This tuning and the comparisons of AOD and  
 255 AVSDs from the assimilation products and WRF-Chem simulations are discussed in detail below.

## 4.2 WRF-Chem code modification

We have corrected the source code of the WRF-Chem v3.7.1 with GOCART aerosol module in several places. These corrections were implemented in the WRF-Chem v4.1.3 official release and will be described in the forthcoming technical publication. Here we briefly discuss the introduced changes and their effects.

260 Firstly, the diagnostic output of PM concentrations was corrected, because contributions of the individual dust and sea salt bins were incorrectly calculated. Therefore,  $\text{PM}_{2.5}$  surface concentrations were erroneously underestimated while  $\text{PM}_{10}$  - were overestimated.

Secondly, we found that the contribution of fine dust particles with radii  $<0.46 \mu\text{m}$  was omitted in the calculation of AOD. This led to an overestimation of the dust emission flux because we force the simulated AOD to match the AERONET observa-  
 265 tions.

Thirdly, we fixed the dust and sea salt gravitational settling subroutine, since initially, the calculations of mass fluxes of settling particles did not account for changes in air density. Due to this error, the total mass of dust and sea salt aerosols increased, violating mass conservation.



## 5 Results

### 270 5.1 Regional climate and circulation

The ME is one of the hottest and driest regions on the Earth. Summer in the ME is long and hot with little precipitation. Precipitation mainly occurs in the south-west of the Arabian Peninsula. Winter is mild, with rainfall being mostly associated with cold fronts and cyclones propagating from the Eastern Mediterranean (Climate.com, 2018). Emission and transport of dust are driven by winds. Emission and deposition of dust are also sensitive to soil moisture and precipitation (Furman, 2003; 275 Shao, 2008; Yu et al., 2015).

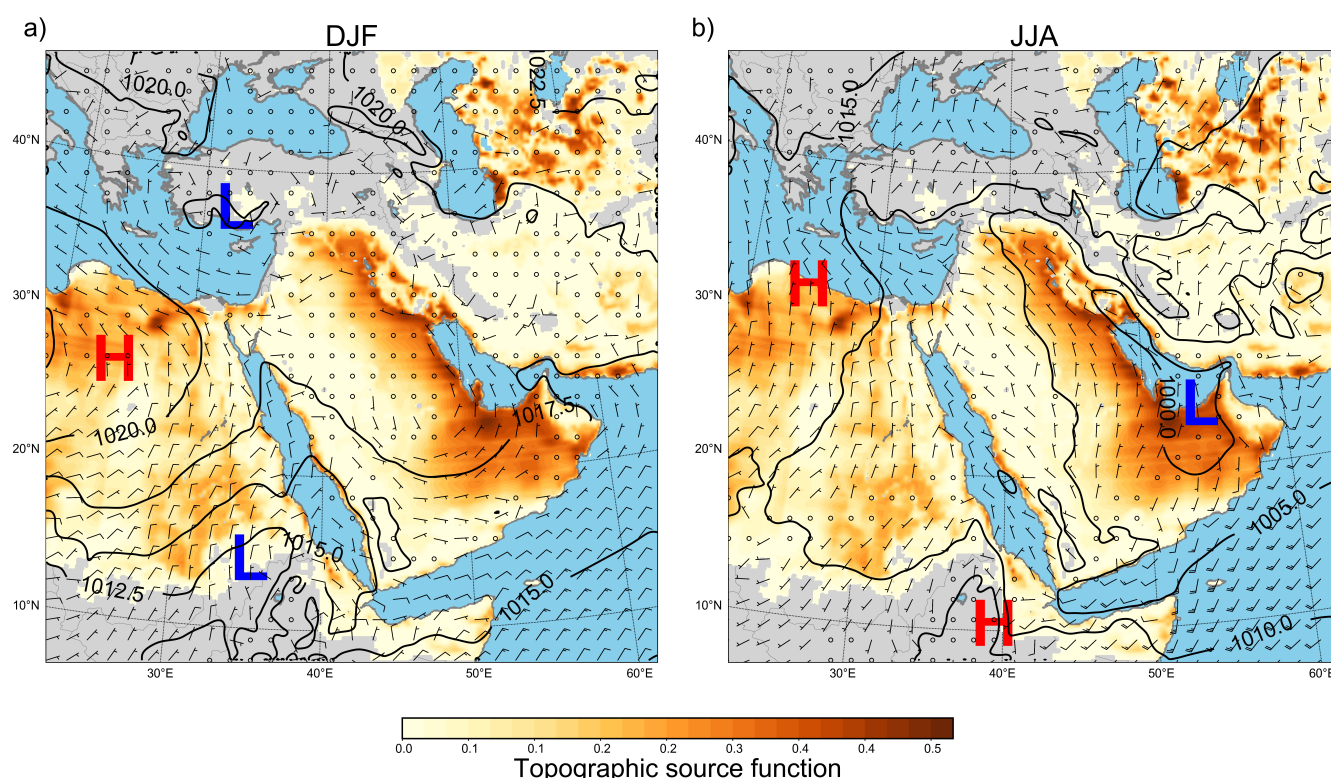


**Figure 2.** Seasonally averaged for 2015-2016 wind barbs (m/s) at 10 m, sea level pressure (contours), and erodibility function (shading) (Ginoux et al., 2001). a) Winter (DJF), b) Summer (JJA).

Figure 2 shows contours of sea level pressure, topographic source function  $S$  (Ginoux et al., 2001), and seasonally 2015-2016 averaged wind speed barbs at 10 m over the ME during winter (DJF) and summer (JJA) from WRF-Chem simulations. Over northeast Africa in winter (see Fig. 2a), the strong pressure gradient between the Red Sea trough and the stationary high-pressure system over Egypt predominantly generates moderate north-easterly winds (up to 10 m/s). Therefore in winter, 280 dust storms occur more frequently in the west of the Arabian Peninsula. Over the Central and Eastern Arabian Peninsula and

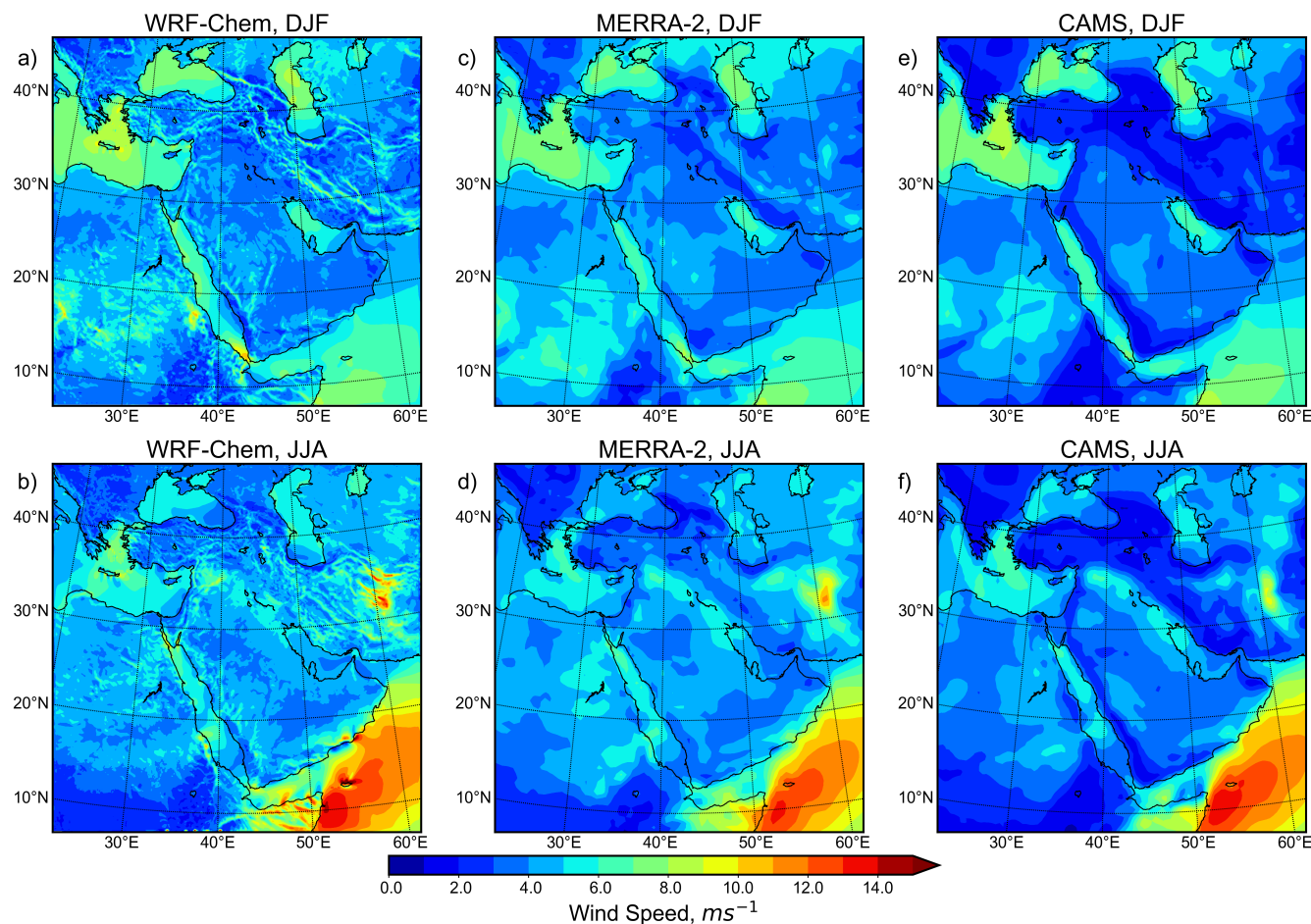


**Figure 3.** Seasonally averaged 2015-2016 wind speed at 10 m for WRF-Chem, MERRA-2, and CAMS-OA during winter (DJF), summer (JJA).

the eastern part of the ME, winds are relatively weak and do not have a clear direction. However, cold fronts generated by Mediterranean cyclones can cause dust storms and dust transport to central regions of the Arabian Peninsula.

In summer (see Fig. 2b the high-pressure system over the eastern Mediterranean and low-pressure system over the Arabian Gulf promote moderate north-northwesterly winds known as *Shamal* (Yu et al., 2016; Hamidi et al., 2013), which dominate  
 285 over the central part of the Arabian peninsula. *Shamal* is the primary driver of dust storm events over this area (Yu et al., 2016; Shao, 2001; Middleton, 1986; Goudie and Middleton, 2006; Notaro et al., 2015). *Shamal* brings dust to the Arabian Gulf, north, and central part of Saudi Arabia, from the Tigris-Euphrates basin of Syria and Iraq (Anisimov et al., 2018).

Figure 3 shows wind speed seasonally averaged for 2015-2016 at 10 m from MERRA-2, CAMS-OA, and WRF-Chem during winter (DJF) and summer (JJA). WRF-Chem spatial distributions of wind speed agree well with MERRA-2 and CAMS-OA,  
 290 but due to the higher spatial resolution, WRF-Chem better resolves the fine-scale spatial structures of the 10 m wind field over



complex terrain. All panels have similar seasonal variations of wind speed. In winter, maximum winds are stronger over the south-east of the domain. In the Central and northern parts of the domain winds are weak. In summer, wind speed increases in the northern and central parts of the ME. *Somali Jet* produces strong (10-15 m/s) winds in the Arabian Sea along the coasts of Somalia and Oman.

295 To conduct the statistical analysis, we interpolated the seasonally averaged 2015-2016 zonal and meridional wind components ( $U$  and  $V$ ) at 10 m from WRF-Chem, and CAMS-OA on MERRA-2 grid and calculated Pearson correlation coefficient ( $R$ ), and root mean square differences ( $RMSD$ ) between each pair, see Tab. 3, correspondingly.  $RMSD$  is calculated using the same formula as the root mean square error ( $RMSE$ ). The procedure of calculation of these parameters is given in Appendix A2. Pearson correlation coefficients provided in Tab. 3 are close to 1. The highest correlation is achieved between  
 300 MERRA-2 and CAMS-OA. WRF-Chem's correlation coefficient with respect to MERRA-2 is smaller but exceeds that of the WRF-Chem - CAMS-OA pair. The WRF-Chem and MERRA-2 wind fields are close partly because WRF-Chem boundary conditions are built using MERRA-2 reanalysis, and the large-scale winds are nudged (see Sec. 4) to the ones from MERRA-2 over the PBL.

The  $RMSDs$  (see Tab. 3) are lower in winter than in summer. All  $RMSDs$  are in the range of 0.45-0.85 m/s. The lowest  
 305  $RMSDs$  are between MERRA-2 and CAMS-OA. Notably, in all three cases, the correlation coefficients for the meridional component  $V$  are higher, and the  $RMSDs$  are lower when compared with the zonal wind component  $U$ . This is because, in summer, the northern winds are stable since they are maintained by the large-scale processes. In contrast, the zonal wind component, which is affected by small-scale processes like sea-breezes, is variable. The results of the statistical analysis in Tab. 3 and the clear similarity of the spatial patterns (among all products) of the averaged 10 m wind fields presented in Fig.  
 310 3, suggest that WRF-Chem captures the magnitude and spatial distribution of the 10 m wind. Thus, we conclude that WRF-Chem with the selected set of physical parameterizations satisfactorily simulates both the large- and meso-scale atmospheric processes in the ME.

**Table 3.** Pearson correlation coefficient  $R$  and root mean square difference  $RMSD$  (m/s) for the seasonally averaged 2015-2016 wind components  $U$  and  $V$  at 10 m.

Season	WRF-Chem wrt CAMS-OA		WRF-Chem wrt MERRA-2		CAMS-OA wrt MERRA-2	
	$R$	$RMSD$	$R$	$RMSD$	$R$	$RMSD$
	$U   V$	$U   V$	$U   V$	$U   V$	$U   V$	$U   V$
Winter (DJF)	0.918   0.954	0.716   0.593	0.954   0.963	0.572   0.537	0.954   0.974	0.558   0.449
Summer (JJA)	0.929   0.981	0.853   0.704	0.938   0.982	0.833   0.669	0.965   0.986	0.636   0.593
Annual mean	0.924   0.968	0.785   0.649	0.946   0.973	0.703   0.603	0.960   0.980	0.597   0.521

\* wrt - with respect to





## 5.2 AOD

In this section, we evaluate the ability of WRF-Chem, CAMS-OA, and MERRA-2 to reproduce the aerosol content in the atmosphere accurately. This content is characterized by AOD. In the ME, mineral dust contribution to the total AOD is dominant ( $\approx 87\%$ ) (Kalenderski and Stenchikov, 2016; Osipov et al., 2015). The treatment of optically active dust within the model is therefore vitally important. AOD is calculated based on aerosol concentrations and aerosol optical properties, which depend upon aerosol size distribution. We, therefore, evaluate how well WRF-Chem and assimilation products reproduce aerosol size distribution.

### 5.2.1 Aerosol size distributions

Dust particles are emitted into the lower atmospheric layer with some predominant size distribution (Kok, 2011). Emitted dust is processed by the atmosphere to produce the atmospheric dust size distribution that is retrieved by the AERONET inversion algorithm (Dubovik and King, 2000) and reported as column integrated AVSD. Strictly speaking, AERONET AVSD incorporates contributions from all types of aerosols. But because dust dominates all other aerosols in the ME, we have to tune the dust emission parameters in the first place.

Eq. (2) assumes that dust particles of different sizes have different emission mass fluxes that are controlled by the  $s_p$  fractions. In WRF-Chem the default values of  $s_p$  fractions for the five dustbins (see Tab. 2) are  $\{0.1, 0.25, 0.25, 0.25, 0.25\}$ . We found that with these default  $s_p$  fractions, WRF-Chem underestimated the volume of fine dust particles in comparison with AERONET AVSD, whereas the coarse mode was overestimated. In combination with the tuning of  $C$  parameter, this led to an overestimation of the total emitted dust mass, since fine particles are optically more efficient per unit mass. To achieve a better agreement between the simulated and AERONET AVSDs we adjusted fractions  $s_p$  to be  $\{0.2, 0.15, 0.17, 0.38, 0.1\}$ . A similar approach was implemented in Khan et al. (2015) using the MADE/SORGAM chemistry/aerosol scheme. Updated  $s_p$  values were kept in further WRF-Chem simulations.

Figure 4 shows seasonally averaged 2015-2016 volume size distributions obtained from MERRA-2, CAMS-OA, AERONET and WRF-Chem with updated  $s_p$  fractions. The comparison is conducted for the *KAUST Campus*, *Mezaira*, *Sede Boker* AERONET sites (see Fig. 1), since only these sites have information on AVSDs during the 2015-2016 period. Because dust bins are coarse, especially in the sub-micron range, model and assimilation products struggle to correctly reproduce the fine mode of the AERONET AVSD (see Fig. 4). The volume size distributions from the model and assimilation products demonstrate pronounced seasonal variability with the increased amount of dust in the atmosphere during spring and summer. Since the *KAUST Campus* and *Mezaira* sites are located in the vicinity of the strong dust sources, the coarse mode at these sites is more pronounced than at the *Sede Boker* site, which is farther from the strong dust emission sources.

Both MERRA-2 and WRF-Chem use the GOCART aerosol scheme with the same five dustbins, and they approximate the shape of the AERONET AVSD relatively well. CAMS-OA uses only three dustbins (see Tab. 2) and fails to reproduce the AERONET AVSD even qualitatively. It overestimates the volume of particles with radii of  $0.55\text{--}0.9\text{ }\mu\text{m}$  and underestimates



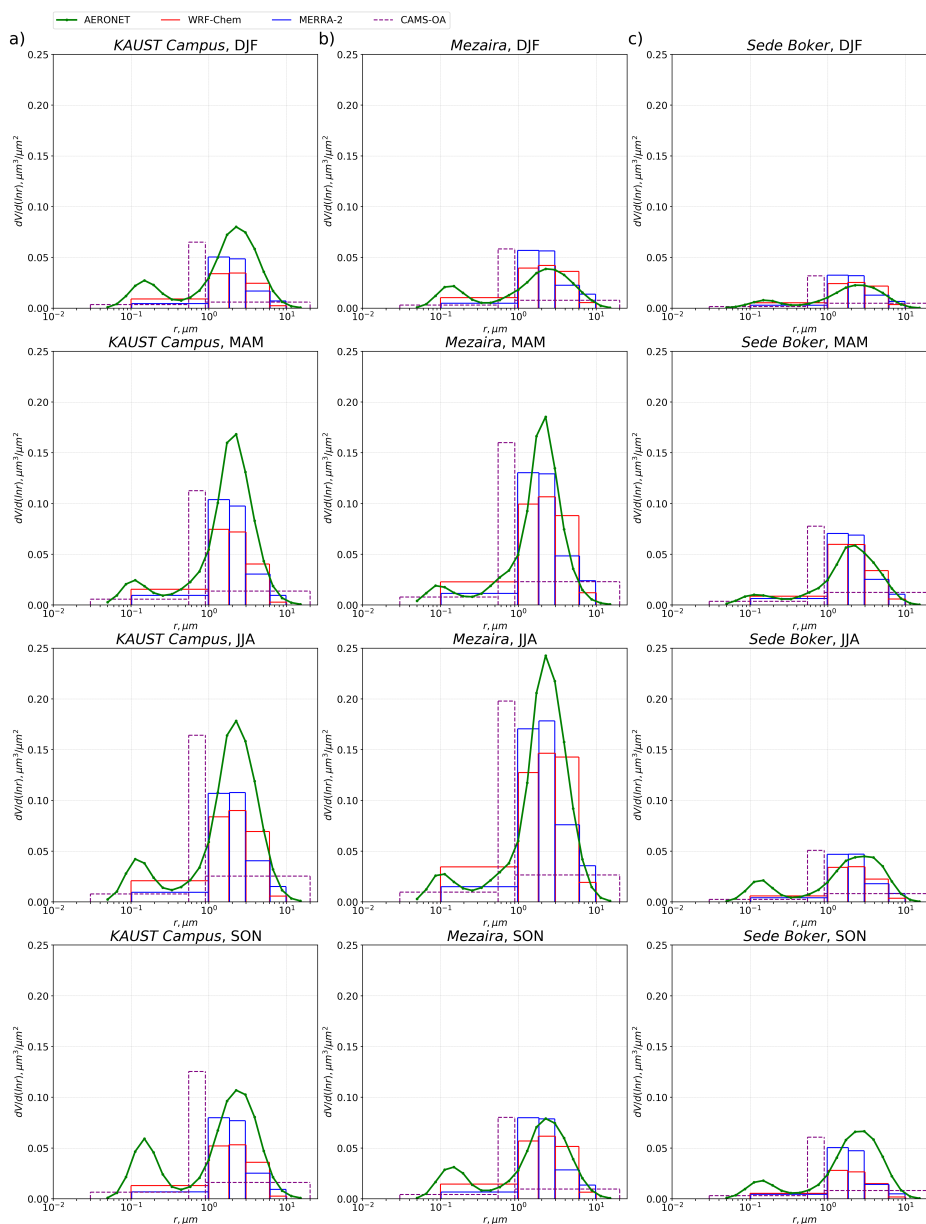


**Figure 4.** Seasonally averaged 2015-2016 AVSDs ( $\mu\text{m}^3/\mu\text{m}^2$ ) obtained from MERRA-2, CAMS-OA, WRF-Chem, and from the AERONET inversion algorithm at a) KAUST Campus, b) Mezaira and c) Sede Boker AERONET sites. Winter (DJF), spring (MAM), summer (JJA) and autumn (SON).

345 the volume of particles with radii of 0.9-20  $\mu\text{m}$ . With the latest system upgrade in 2019, this weakness of CAMS-OA has been corrected by introducing of a new dust scheme (Nabat et al., 2012).

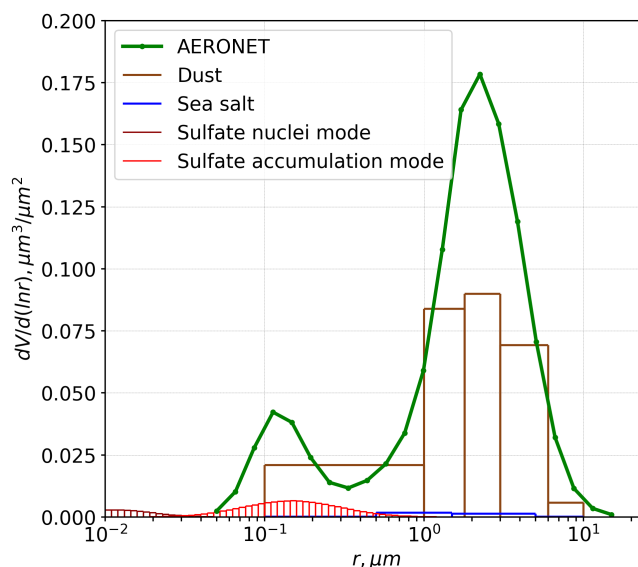


**Figure 5.** Summer (JJA) averaged 2015-2016 AVSD ( $\mu\text{m}^3/\mu\text{m}^2$ ) at *KAUST Campus* AERONET site obtained from the AERONET inversion algorithm and from WRF-Chem.

The fine mode in the AERONET AVSD is more pronounced at the *KAUST Campus* in comparison with the other AERONET sites due to its proximity to strong  $\text{SO}_2$  sources located along the west coast of Saudi Arabia. This proximity leads to a higher contribution of fine sulfate particles to the fine mode. The smaller volume of fine particles in the WRF-Chem and MERRA-2 simulated dust AVSD (see Fig. 4) is in part because the sulfate contribution is not shown. Sea salt particles/droplets are relatively large and mostly contribute to the coarse mode.

Figure 5 shows the contributions of dust, sea salt, and sulfate aerosols into the AVSD at the *KAUST Campus* AERONET site in WRF-Chem simulation averaged for two summer seasons (JJA) of 2015-2016. In WRF-Chem, sulfate aerosol is computed using a bulk approach. However, for calculating of aerosol optical properties, it is assumed that sulfate aerosol is described by two log-normal modes: nuclei and accumulation. According to WRF-Chem source code, the nuclei mode radii  $\mu_{\text{nuc}}=0.005 \mu\text{m}$  and geometric width  $\sigma_{\text{nuc}}=1.7$ , the accumulation mode radii  $\mu_{\text{acc}}=0.035 \mu\text{m}$  and geometric width  $\sigma_{\text{acc}}=2.0$ . The nuclei mode comprises 25% of the sulfate aerosol mass, and accumulation mode - 75%. It is assumed that sulfate aerosol density is  $1800 \text{ kg/m}^3$  and sea salt density is  $2200 \text{ kg/m}^3$ . Figure 5 demonstrates that the contribution of the sulfate nuclei mode in the aerosol volume is almost negligible, while the sulfate accumulation mode adds in the volume of aerosol particles with radii  $<1 \mu\text{m}$ . The contribution of the sea salt aerosol into AVSD in WRF-Chem simulations is very little.

### 5.2.2 Comparison with AERONET AOD

The comparison of the daily averaged AOD from WRF-Chem, MERRA-2, CAMS-OA, MODIS-DB&DT, and MAIAC with AERONET AOD observations conducted at *KAUST Campus*, *Mezaira* and *Sede Boker* during 2015-2016 period is presented

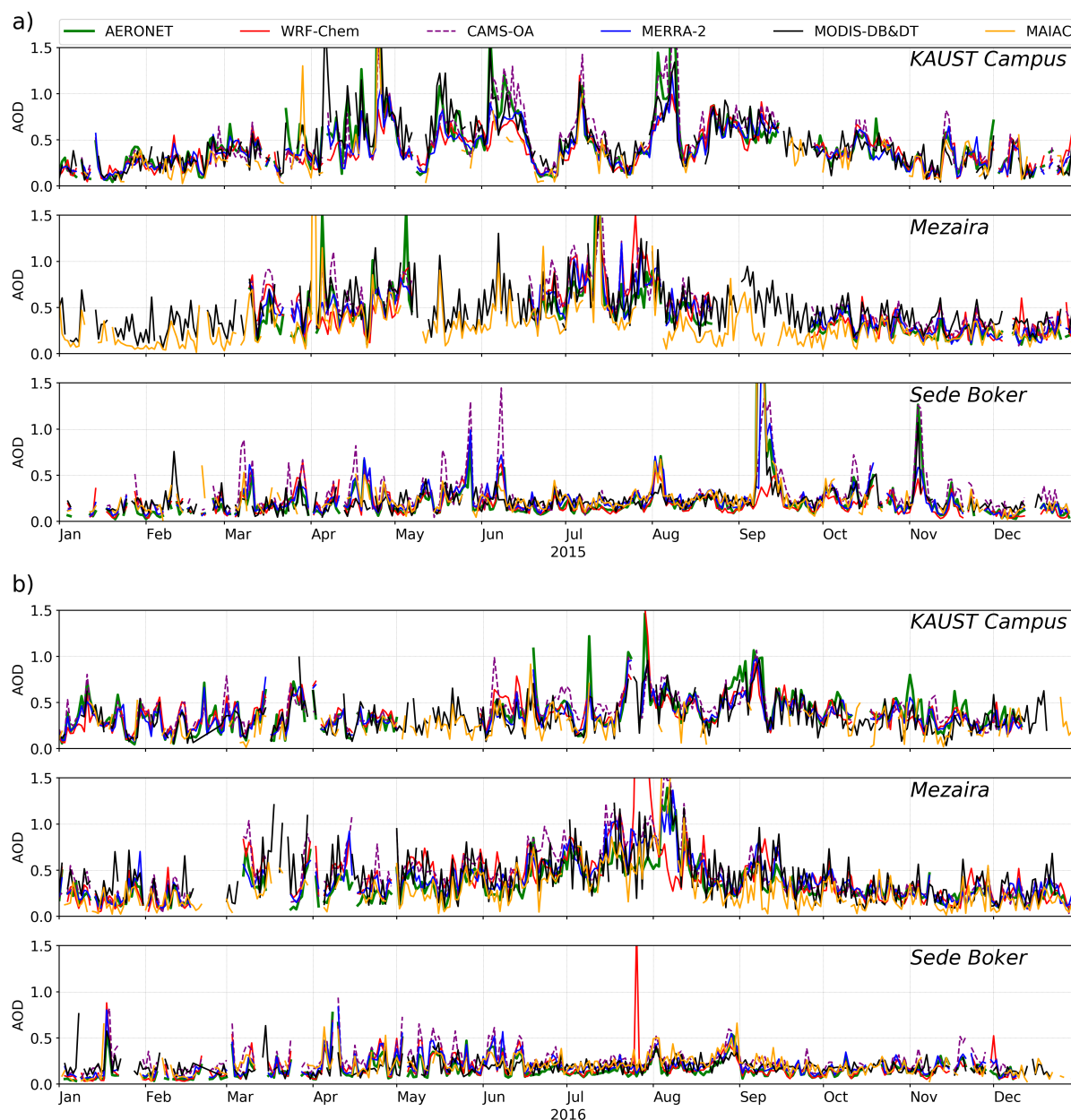


**Figure 6.** Daily averaged AOD 2015-2016 at three AERONET sites (*KAUST Campus*, *Mezaira*, *Sede Boker*) computed for WRF-Chem, AERONET, MERRA-2, CAMS-OA, MODIS-DB&DT, and MAIAC.

in Fig. 6. Because AERONET conducts observations only during the daylight time, we interpolated WRF-Chem, MERRA-2,  
 365 CAMS-OA AODs to the AERONET measurements times and then conducted time averaging to make simulated and observed



**Table 4.** Pearson correlation coefficient  $R$  and mean  $BIAS$  calculated for daily averaged AOD time-series from WRF-Chem, CAMS-OA, MERRA-2, MODIS-DB&DT, and MAIAC with respect to AERONET AOD observations.

	WRF-Chem		CAMS-OA		MERRA-2		MODIS-DB&DT		MAIAC	
	$BIAS$	$R$	$BIAS$	$R$	$BIAS$	$R$	$BIAS$	$R$	$BIAS$	$R$
	2015									
<i>KAUST Campus</i>	-0.05	0.73	0.01	0.86	-0.05	0.85	0.02	0.83	-0.07	0.88
<i>Mezaira</i>	0.05	0.73	0.11	0.80	0.03	0.83	0.10	0.78	-0.07	0.88
<i>Sede Boker</i>	-0.03	0.44	0.07	0.65	0.02	0.72	0.02	0.92	0.04	0.96
	2016									
<i>KAUST Campus</i>	0.00	0.60	0.01	0.76	-0.03	0.88	-0.05	0.77	-0.07	0.64
<i>Mezaira</i>	0.09	0.52	0.11	0.88	0.06	0.87	0.08	0.70	-0.04	0.83
<i>Sede Boker</i>	0.02	0.66	0.10	0.84	0.04	0.91	0.03	0.47	0.05	0.63

AODs consistent. AODs from MODIS-DB&DT and MAIAC are provided as a daily average. However, MODIS conducts observations only twice a day during daylight time.

The model and assimilation products reproduce the magnitude and temporal evolution of the observed AERONET AOD at all sites quite well. During both years, *KAUST Campus* and *Mezaira* sites show higher AOD in summer and lower AOD in winter.

To quantify the capability of the WRF-Chem, MERRA-2, and CAMS-OA models, and the MODIS-DB&DT and MAIAC products to reproduce the AERONET AOD, we calculate Pearson correlation coefficient  $R$  and mean  $BIAS$  (see Appendix A2) with respect to the AERONET AOD observations for the 2015-2016 period, see Tab. 4. The correlation coefficients are the highest for MERRA-2 and MAIAC. MAIAC shows better correlation than MERRA-2 during 2015 (0.88-0.96), but MERRA-2 is better correlated with AERONET (0.88-0.91) than MAIAC in 2016. CAMS-OA, despite it does not assimilate AERONET, shows better correlations (0.65-0.88) than MODIS-DB&DT (0.47-0.92). However, CAMS-OA overestimates AOD, particularly during acute dust events, and has a relatively high positive mean  $BIAS$ . The  $R$  coefficient for the WRF-Chem AOD is (0.44-0.73). MERRA-2 and WRF-Chem have the lowest  $BIAS$  in comparison with the other models and products. Both MODIS-DB&DT and MAIAC have a slightly larger  $BIAS$  than WRF-Chem. MODIS-DB&DT  $BIAS$  is positive except *KAUST Campus* in 2016, while MAIAC  $BIAS$  is negative for *KAUST Campus* and *Mezaira* and positive for *Sede Boker* during both years (see Tab. 4).

### 5.2.3 Comparison of spatial AOD distributions

We also examine how well MERRA-2, CAMS-OA, MAIAC, and WRF-Chem reproduce spatial patterns and seasonal variability of the AOD in comparison with MODIS-DB&DT retrievals. The seasonally and annually-averaged 2015-2016 AOD fields from WRF-Chem, CAMS-OA, MERRA-2, and the two MODIS retrievals DB&DT and MAIAC are presented in Fig. 7.

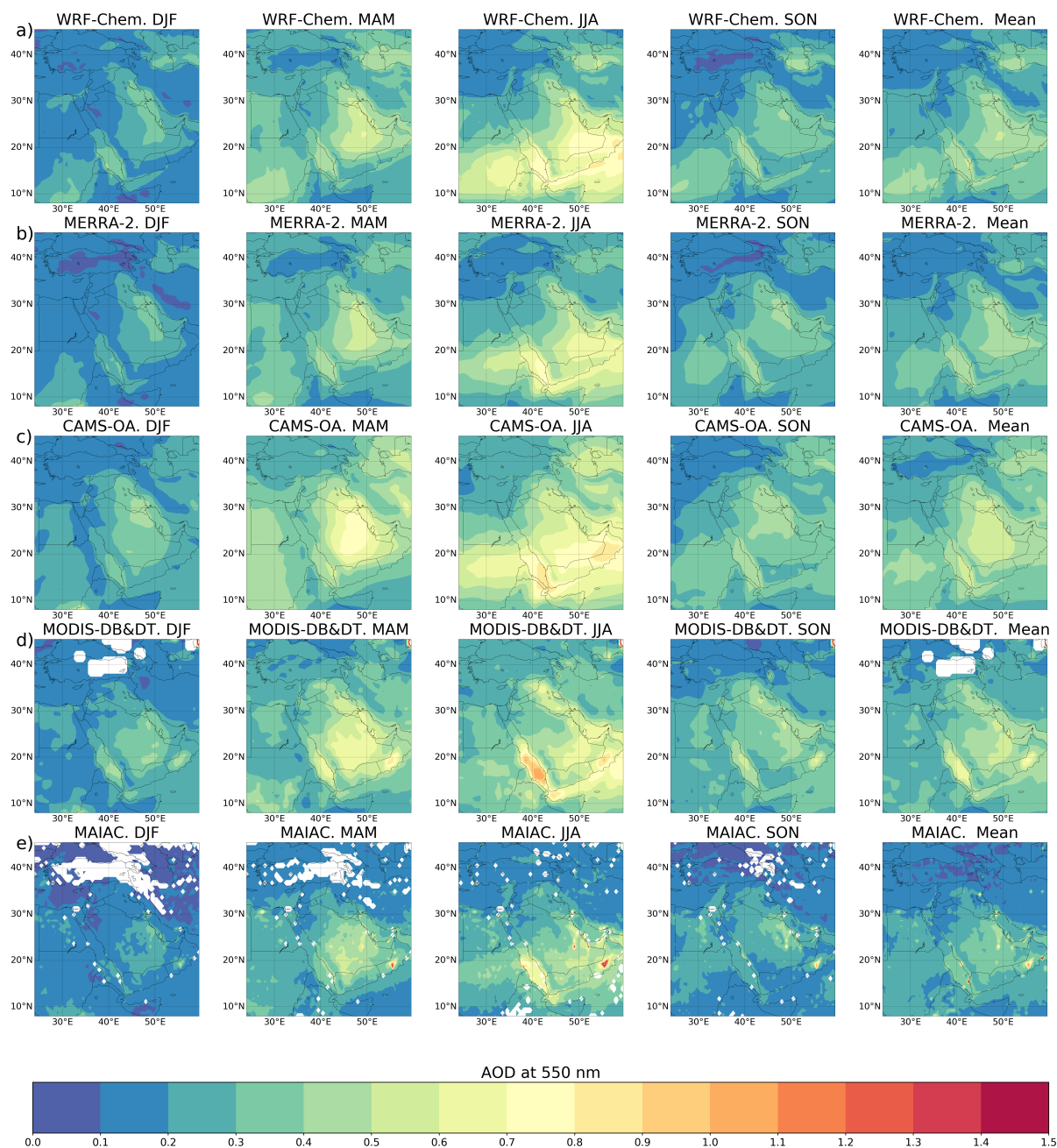


**Figure 7.** Seasonally averaged 2015-2016 AOD. Right column is annual mean AOD. Rows: a) WRF-Chem, b) MERRA-2, c) CAMS-OA, d) MODIS-DB&DT, and e) MAIAC. Winter (DJF), spring (MAM), summer (JJA), and autumn (SON). White dots are NaN values.

For the comparison, we interpolate AOD fields (preserving the area average AODs) on the MERRA-2 grid and calculate the Pearson correlation coefficient  $R$  and root mean square error  $RMSE$  (see Tab. 5) with respect to MODIS-DB&DT AOD.



The spatial and seasonal variability of the AOD from WRF-Chem, CAMS-OA, MERRA-2, and MAIAC is in good agreement with the MODIS-DB&DT AOD. The WRF-Chem and assimilation products exhibit similar AOD patterns. MAIAC underestimates AOD over the whole domain during all seasons in comparison with MODIS-DB&DT, which is consistent with the MAIAC and MODIS-DB&DT AOD comparison with AERONET AOD (see Fig. 6). CAMS-OA overestimates MODIS-DB&DT AOD in spring and summer but has the best agreement with MODIS-DB&DT in autumn and winter. In summer, when dust emission is at its maximum, WRF-Chem shows higher AOD over the south-eastern part of the Arabian Peninsula in comparison with MODIS-DB&DT AOD, but MERRA-2 underestimates MODIS-DB&DT AOD in summer. In winter and autumn, WRF-Chem and MERRA-2 demonstrate similar patterns and AOD levels, but both of them slightly underestimate MODIS-DB&DT AOD. The extremely high MODIS-DB&DT AOD over the southern part of the Red Sea is real but is overestimated in comparison with the findings of Brindley et al. (2015); Osipov and Stenchikov (2018).

When conducting statistical analysis, the grid-cells with NAN-values in MODIS-DB&DT and MAIAC retrievals were excluded from the analysis both in observations and the model outputs. The statistical scores provided in Tab. 5 show that the annual mean AOD from MERRA-2 and CAMS-OA have the highest spatial correlations (0.720 and 0.696) and one of the lowest *RMSE* (0.088 and 0.093) with respect to MODIS-DB&DT AOD, followed by WRF-Chem ( $R=0.653$ ,  $RMSE=0.090$ ) and MAIAC AOD, which has the lowest correlation (0.608) and highest *RMSE* (0.135). Notably, the difference in terms of *R* and *RMSE* between the two retrieval algorithms MODIS-DB&DT and MAIAC is bigger than the difference between WRF-Chem and MODIS-DB&DT.

**Table 5.** Pearson correlation coefficient (*R*) and root mean square error (*RMSE*) calculated for seasonally and annually averaged 2015-2016 AOD geographic distributions from CAMS-OA, MAIAC, MERRA-2, and WRF-Chem with respect to MODIS-DB&DT AOD.

	CAMS-OA		MAIAC		MERRA-2		WRF-Chem	
	<i>R</i>	<i>RMSE</i>	<i>R</i>	<i>RMSE</i>	<i>R</i>	<i>RMSE</i>	<i>R</i>	<i>RMSE</i>
Winter (DJF)	0.625	0.074	0.459	0.109	0.577	0.078	0.464	0.082
Spring (MAM)	0.726	0.112	0.526	0.180	0.742	0.102	0.670	0.103
Summer (JJA)	0.737	0.142	0.601	0.190	0.792	0.112	0.747	0.128
Autumn (SON)	0.620	0.085	0.455	0.140	0.647	0.087	0.539	0.098
Annual mean	0.696	0.093	0.608	0.135	0.720	0.088	0.653	0.090

Based on the comparison of WRF-Chem AOD with the AOD from AERONET and MODIS observations, we conclude that spatial and temporal WRF-Chem's AOD distribution is in good agreement with the available ground-based and satellite observations.

### 5.3 Air-quality

To test the ability of the data assimilation products and models to characterize air-quality in the ME, we compare surface daily mean  $PM_{2.5}$  and  $PM_{10}$  concentrations from WRF-Chem, MERRA-2, and CAMS-OA, with daily averaged measurements





conducted by the three AQMS, see Fig. 8 and 9. The AQMS are installed in Jeddah, Riyadh, and Dammam (Fig. 1), the Saudi Arabian mega-cities. PM measurements conducted by MODON (see Sec. 2.3) are only available starting from 2016. The modeled  $PM_{2.5}$  and  $PM_{10}$  concentrations were sampled from the model fields at the exact AQMS locations. The following formulas were used to calculate  $PM_{2.5}$  and  $PM_{10}$  surface concentrations using WRF-Chem and MERRA-2 output:

$$\begin{aligned}
 415 \quad PM_{2.5} &= DUST_1 + DUST_2 * 0.38 + SEAS_2 + SEAS_3 * 0.83 \\
 &\quad + sulfate + (OC_1 + OC_2) * OC_{mfac} + BC_1 + BC_2 \\
 PM_{10} &= DUST_1 + DUST_2 + DUST_3 + DUST_4 * 0.74 + SEAS_2 + SEAS_3 + SEAS_4 \\
 &\quad + sulfate + (OC_1 + OC_2) * OC_{mfac} + BC_1 + BC_2
 \end{aligned} \tag{4}$$

where  $DUST_{1,2,3,4}$ ,  $SEAS_{2,3,4}$ ,  $OC_{1,2}$ ,  $BC_{1,2}$ , and *sulfate* are respectively the concentrations of the dust in the first four  
 420 bins, sea-salt in the three bins, organic and black carbon (hydrophobic and hydrophilic) and sulfate ion ( $SO_4^{2-}$ ). The factor  $OC_{mfac} = 1.8$  accounts for the conversion of organic carbon into organic matter. WRF-Chem simulates only the last four sea salt bins from the GOCART model (see Tab. 2). Because the first sea salt bin is poorly populated, we omit it from calculations of PM for MERRA-2.

CAMS-OA  $PM_{2.5}$  and  $PM_{10}$  were calculated using the following relations ([https://confluence.ecmwf.int/display/CUSF/](https://confluence.ecmwf.int/display/CUSF/PM10+and+PM25+global+products)  
 425  $PM_{10}$ +and+ $PM_{25}$ +global+products):

$$\begin{aligned}
 PM_{2.5} &= DD_1 + DD_2 + SS_1/4.3 + 0.5 * SS_2/4.3 \\
 &\quad + 0.7 * (OM_1 + OM_2 + sulfate) + BC_1 + BC_2 \\
 PM_{10} &= DD_1 + DD_2 + DD_3 * 0.4 + SS_1/4.3 + SS_2/4.3 \\
 &\quad + OM_1 + OM_2 + sulfate + BC_1 + BC_2
 \end{aligned} \tag{5}$$

430 where  $DD_{1,2,3}$ ,  $SS_{1,2}$ , *sulfate*,  $BC_{1,2}$ ,  $OM_{1,2}$  are surface concentration of dust in three bins, sea salt in two bins, sulfate, black carbon, and organic matter (hydrophobic and hydrophilic). The size ranges of dust and sea salt bins from CAMS-OA are presented in Tab. 2.

The histograms at the right-side panels in Fig. 8 and 9 show the annual mean PM concentrations from WRF-Chem, MERRA-2, and CAMS-OA split into the dust and non-dust components. We also calculated the separate contributions of sulfate, sea salt,  
 435 organic matter, and black carbon into the non-dust  $PM_{2.5}$  and  $PM_{10}$ , see Tab. 6 and 7, respectively. The dashed and dash-dotted horizontal lines correspond to KSA-PME limits and WHO air quality guidelines for daily (on the left-side panels) and annual mean (on the right-side panels) PM concentrations.

The sporadic peaks in the observations which are not captured by the model and assimilation products are due to unaccounted factors, such as nearby traffic, construction works, and local anthropogenic or natural emissions, which are not present in the  
 440 emission inventories, or due to meteorological fluctuations that are not resolved in the models. Talking about extreme dust pollution cases, we analyzed dust surface concentrations using WRF-Chem output during the dust storm, which took place in



the Jeddah region on 8th July in 2016. The calculated surface concentrations in all dustbins  $DUST_{1,2,3,4,5}$  at the peak of the storm were  $\{55, 58, 63, 111, 11\} \mu\text{g}/\text{m}^3$ , respectively. The sum of all dustbins yields the total dust concentration of  $298 \mu\text{g}/\text{m}^3$ .

### 5.3.1 $\text{PM}_{2.5}$

445 Fig. 8 shows that the daily averaged  $\text{PM}_{2.5}$  concentrations observed by MODON AQMS at all locations never drop below the WHO limit of  $25 \mu\text{g}/\text{m}^3$ . During the severe dust events, this limit is exceeded in 2016 10-15 times. The less restrictive KSA-PME limit of  $35 \mu\text{g}/\text{m}^3$  is exceeded 7-11 times during the dust outbreaks. Annually averaged MODON measurements are 8-18 times higher than the  $10 \mu\text{g}/\text{m}^3$  WHO limit and 5-12 times higher than the  $15 \mu\text{g}/\text{m}^3$  KSA-PME limit for annual mean  $\text{PM}_{2.5}$  concentrations.

450 Both data assimilation products and WRF-Chem underestimate annual mean  $\text{PM}_{2.5}$  concentrations in Jeddah and Riyadh and slightly overestimate  $\text{PM}_{2.5}$  in Dammam in comparison with observed concentrations during 2016. The CAMS-OA annual mean surface  $\text{PM}_{2.5}$  concentrations in Jeddah and Riyadh are higher than those from WRF-Chem and MERRA-2, providing the best fit for MODON observations, at least on an annual mean (during 2016) basis.

Annual mean  $\text{PM}_{2.5}$  concentrations from WRF-Chem and MERRA-2 exceed the WHO limit of  $10 \mu\text{g}/\text{m}^3$  5 and 11 times, 455 respectively, in all locations. The KSA-PME limit of  $15 \mu\text{g}/\text{m}^3$  for annual average  $\text{PM}_{2.5}$  concentrations is exceeded 3-8 times, respectively, for WRF-Chem and MERRA-2. In Jeddah and Dammam, WRF-Chem and MERRA-2 show similar contributions of non-dust components to  $\text{PM}_{2.5}$  (25-33% in Jeddah and 10-14% in Dammam), but in MERRA-2 sea salt is a major contributor into non-dust  $\text{PM}_{2.5}$ , while in WRF-Chem it is sulfate, see Tab. 6. This difference between WRF-Chem and MERRA-2 is mainly because MERRA-2 generates more sea salt, but also because MERRA-2 underestimates  $\text{SO}_2$  emissions located in the 460 Arabian Gulf and along the west coast of Saudi Arabia (Janssens-Maenhout et al., 2013), and hence underestimates sulfate concentrations, as discussed in Sec. 4.1. In Riyadh, the contribution of the non-dust component to  $\text{PM}_{2.5}$  is  $\approx 9$ -11% for both MERRA-2 and WRF-Chem. In CAMS-OA, the contribution of non-dust particulates to  $\text{PM}_{2.5}$  in Jeddah and Dammam is  $\approx 7$ -11%, and the contribution of sea salt is little. According to Tab. 6, in all considered cities, the contribution of black carbon to  $\text{PM}_{2.5}$  is not significant in WRF-Chem, CAMS-OA, and MERRA-2. In MERRA-2, the contribution of organic matter to 465  $\text{PM}_{2.5}$  is more substantial (but still minor) in comparison with WRF-Chem and CAMS-OA.

### 5.3.2 $\text{PM}_{10}$

Daily averaged MODON measurements almost continuously exceed the WHO guideline of  $50 \mu\text{g}/\text{m}^3$  at all locations. In Riyadh and Dammam,  $\text{PM}_{10}$  concentration is higher than in Jeddah, where the KSA-PME limit of  $340 \mu\text{g}/\text{m}^3$  for daily averaged  $\text{PM}_{10}$  is exceeded in 2016 about a dozen times. In Dammam, this limit is more frequently exceeded, especially 470 during the summer period. During acute dust events in Dammam, daily averaged  $\text{PM}_{10}$  concentrations can exceed the WHO guideline limit by more than 10-20 times. Annually averaged MODON measurements are 8-11 times higher than the  $20 \mu\text{g}/\text{m}^3$  WHO guideline, and in 2-3 times higher than the  $80 \mu\text{g}/\text{m}^3$  KSA-PME limits for annual mean  $\text{PM}_{10}$  concentrations.

WRF-Chem simulations, MERRA-2, and CAMS-OA data assimilation products compare well with  $\text{PM}_{10}$  observations by MODON in Jeddah and Riyadh. The MERRA-2 and WRF-Chem  $\text{PM}_{10}$  concentrations time-series are quite close to each



**Figure 8.** Left: WRF-Chem daily averaged  $\text{PM}_{2.5}$  surface concentrations ( $\mu\text{g}/\text{m}^3$ ) with MODON observations, MERRA-2, CAMS-OA at Jeddah, Riyadh, Dammam. The dash-dotted line corresponds to the  $25 \mu\text{g}/\text{m}^3$  WHO daily average guideline. Right: stacked bars show the decomposition of the  $\text{PM}_{2.5}$  annual mean surface concentrations into dust and non-dust components. The dash-dotted line corresponds to the  $10 \mu\text{g}/\text{m}^3$  WHO annual guideline. Numbers on the right hand side of WRF-Chem, CAMS-OA, and MERRA-2 bars show the contribution (%) of the dust and non-dust into the total  $\text{PM}_{2.5}$  concentration. a) 2015, b) 2016.

other. Both WRF-Chem and MERRA-2 overestimate observations in Dammam. WRF-Chem reproduces annually-averaged MODON  $\text{PM}_{10}$  observations quite well, especially in Jeddah and Riyadh.



**Table 6.** Contributions (%) of dust and non-dust components into  $PM_{2.5}$  for Jeddah, Riyadh, and Dammam during 2015-2016.

	Jeddah			Riyadh			Dammam		
	WRF-Chem	CAMS-OA	MERRA-2	WRF-Chem	CAMS-OA	MERRA-2	WRF-Chem	CAMS-OA	MERRA-2
	2015								
dust	74.8	90.9	70.6	91.1	96.8	90.8	90.2	93.0	88.1
sulf	15.6	5.1	6.1	6.8	2.1	5.0	7.5	3.9	3.6
BC	1.7	0.7	0.6	0.1	0.2	0.3	0.1	0.7	0.3
OM	3.3	3.1	5.1	1.4	0.8	2.7	1.2	2.3	3.1
salt	4.5	0.1	17.6	0.7	0.1	1.3	1.0	0.1	4.9
	2016								
dust	71.9	89.9	66.8	90.6	96.8	89.6	89.1	90.9	85.5
sulf	18.9	5.7	6.8	7.0	1.9	5.7	8.4	4.7	4.3
BC	1.7	0.8	0.7	0.1	0.3	0.3	0.1	0.9	0.4
OM	3.2	3.4	5.4	1.6	0.9	2.9	1.3	3.4	4.1
salt	4.4	0.1	20.4	0.7	0.1	1.4	1.1	0.1	5.7

\* for WRF-Chem and MERRA-2:  $dust = DUST_1 + DUST_2 * 0.38$ ,  $BC = BC_1 + BC_2$ ,  $sulf = sulfate$ ,  $OM = (OC_1 + OC_2) * OC_{mac}$ ,  
 $salt = SS_2 + SS_3 * 0.83$

\*\*for CAMS:  $dust = DD_1 + DD_2$ ,  $sulf = 0.7 * sulfate$ ,  $BC = BC_1 + BC_2$ ,  $OM = 0.7 * (OM_1 + OM_2)$ ,  
 $salt = SS_1 / 4.3 + 0.5 * SS_2 / 4.3$

Abbreviations of the aerosols' names correspond to those given in Sec. 5.3.

CAMS-OA, in general, underestimates  $PM_{10}$  concentrations in comparison with the observations. This is in agreement with Cuevas et al. (2014), who stated that MACC (the predecessor of CAMS-OA) underestimates  $PM_{10}$  daily and monthly means all year long, and with our findings in Sec. 5.2.1, where we have shown that CAMS-OA underestimates the volume of particles with radii 0.9-20  $\mu m$ .

According to Tab. 7 MERRA-2 shows the highest contribution of the sea salt into  $PM_{10}$  in the coastal cities of Jeddah and Dammam. MERRA-2 demonstrates the lowest ( $\approx 1-2\%$ ) contribution of sulfate to  $PM_{10}$ , while WRF-Chem and CAMS-OA produce similar sulfate contribution to  $PM_{10}$  in Jeddah ( $\approx 6\%$ ) and Riyadh ( $\approx 2\%$ ). MERRA-2 also shows the lowest contribution ( $\approx 0.1-0.2\%$ ) of black carbon to  $PM_{10}$  in all considered cities. CAMS-OA organic matter contribution to  $PM_{10}$  is prevailing (up to 3-4 times) over the WRF-Chem and MERRA-2 contributions.

### 5.3.3 Spatial patterns of air-pollution

As we have shown, WRF-Chem provides reliable estimates of aerosol pollution in major Saudi Arabia's cities, Riyadh, Jeddah, and Dammam. Further, we will use WRF-Chem output averaged for 2015-2016 to discuss the spatial patterns of aerosol pollution and partial contributions from natural and anthropogenic aerosols into PM.

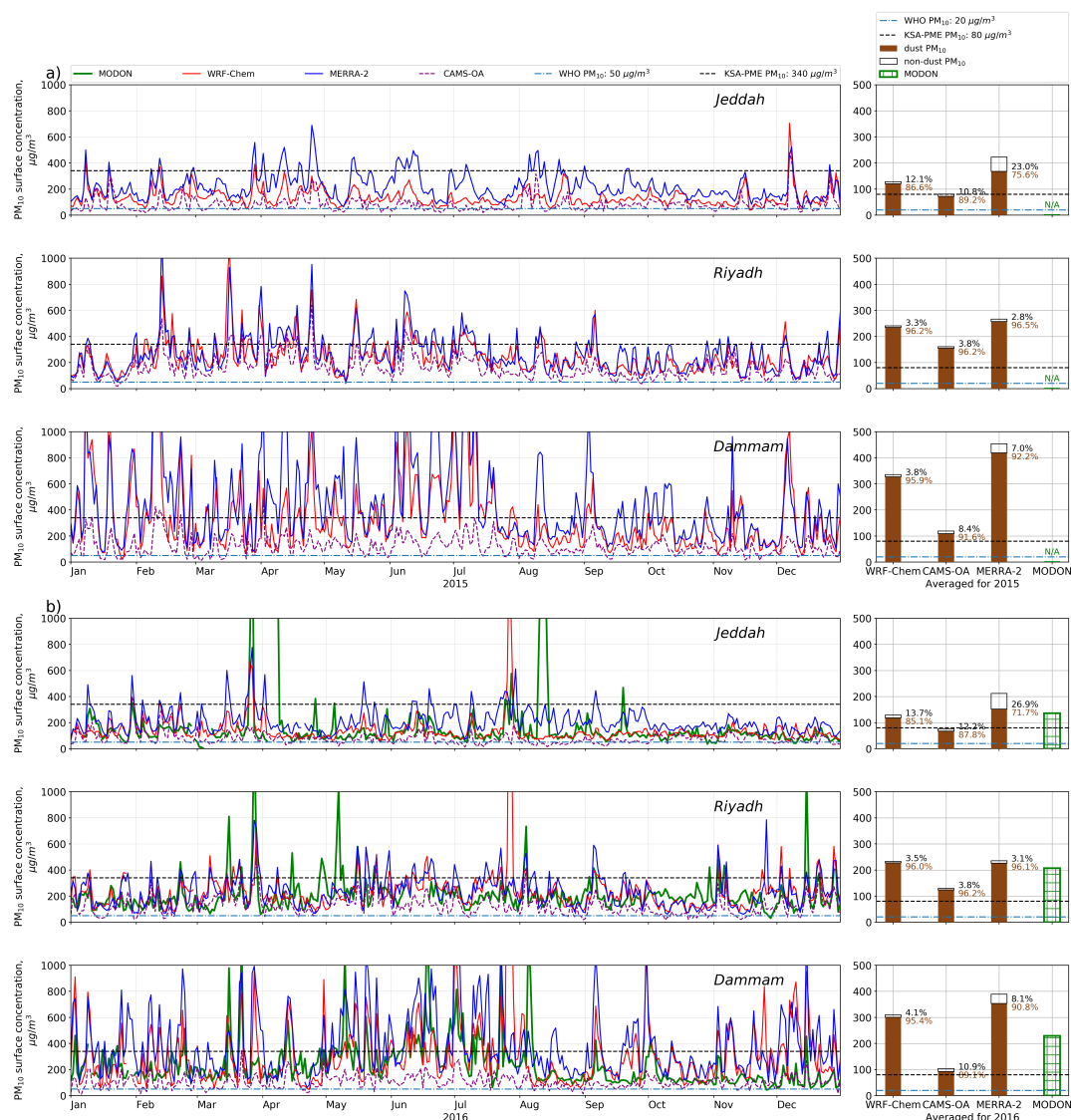


**Figure 9.** Left: WRF-Chem daily averaged  $\text{PM}_{10}$  surface concentrations ( $\mu\text{g}/\text{m}^3$ ) with the MODON observations and MERRA-2 and CAMS-OA, at Jeddah, Riyadh, and Dammam. The dash-dotted line corresponds to the 50  $\mu\text{g}/\text{m}^3$  WHO daily - guideline. Right: stacked bars show the decomposition of the  $\text{PM}_{10}$  annual mean surface concentrations into dust and non-dust components. The dash-dotted line corresponds to the 20  $\mu\text{g}/\text{m}^3$  WHO annual guideline. Numbers on the right-hand side of WRF-Chem, CAMS-OA, and MERRA-2 bars show the contribution (%) of the dust and non-dust particulates to the total  $\text{PM}_{10}$  concentration. a) 2015, b) 2016 year.

Figures 10 a, b, c show the spatial distributions of the  $\text{PM}_{2.5}$  and  $\text{PM}_{10}$  surface concentrations and the  $\text{PM}_{2.5}/\text{PM}_{10}$  ratio. The left limits of the color bars for  $\text{PM}_{2.5}$  and  $\text{PM}_{10}$  are set to be equal to the corresponding WHO annual guideline limits. Over the whole domain, the annual mean surface concentrations of  $\text{PM}_{2.5}$  and  $\text{PM}_{10}$  exceed WHO guidelines of 10 and 20



**Table 7.** Contributions (%) of dust and non-dust components into PM<sub>10</sub> for Jeddah, Riyadh, and Dammam during 2015-2016.

	Jeddah			Riyadh			Dammam		
	WRF-Chem	CAMS-OA	MERRA-2	WRF-Chem	CAMS-OA	MERRA-2	WRF-Chem	CAMS-OA	MERRA-2
2015									
<i>dust</i>	86.6	89.2	75.6	96.2	96.2	96.5	95.9	91.6	92.2
<i>sulf</i>	6.0	6.2	1.7	2.3	2.6	1.4	2.5	4.8	0.9
<i>BC</i>	1.9	0.6	0.2	0.5	0.2	0.1	0.4	0.6	0.1
<i>OM</i>	1.3	3.8	1.4	0.5	1.0	0.7	0.4	2.8	0.8
<i>salt</i>	4.2	0.2	21.2	0.5	0.1	1.4	0.8	0.2	6.0
2016									
<i>dust</i>	85.1	87.8	71.7	96.0	96.2	96.1	95.4	89.1	90.8
<i>sulf</i>	7.5	7.0	1.9	2.4	2.3	1.6	2.8	5.7	1.1
<i>BC</i>	1.9	0.7	0.2	0.6	0.2	0.1	0.5	0.8	0.1
<i>OM</i>	1.3	4.2	1.5	0.5	1.1	0.8	0.4	4.2	1.1
<i>salt</i>	4.3	0.2	24.8	0.5	0.1	1.5	0.9	0.2	6.8

\* for WRF-Chem and MERRA-2:  $dust = DUST_1 + DUST_2 + DUST_3 + DUST_4 * 0.74$ ,  $sulf = sulfate$ ,  $BC = BC_1 + BC_2$ ,

$OM = (OC_1 + OC_2) * OC_{mfac}$ ,  $salt = SS_2 + SS_3 + SS_4$

\*\*for CAMS:  $dust = DD_1 + DD_2 + DD_3 * 0.4$ ,  $sulf = sulfate$ ,  $BC = BC_1 + BC_2$ ,  $OM = OM_1 + OM_2$ ,  $salt = SS_1/4.3 + SS_2/4.3$

Abbreviations of the aerosols' names correspond to those given in Sec. 5.3.

µg/m<sup>3</sup>, correspondingly. The regions of high surface concentrations coincide with the main dust sources, which span from Northern Iraq to Oman, include Sudan, Egypt, Algeria, and Turkmenistan. PM concentrations in these regions exceed even the less restrictive KSA-PME air quality limit for annual mean PM<sub>2.5</sub> and PM<sub>10</sub> concentrations by more than 5 times.

In the entire domain, the max, min, and mean values of the PM<sub>2.5</sub>/PM<sub>10</sub> ratio (see Fig. 10c) are 0.89, 0.24, and 0.38 respectively. As expected, the lower PM<sub>2.5</sub>/PM<sub>10</sub> ratios (0.2-0.3) are observed over the dust source regions (i.e., along the eastern Arabian peninsula, Iraq, and northern Africa), where both coarse and fine particles are generated. However, large particles can not be transported as far from source regions as small particles, due to the shorter lifetime of large particles compared with small particles with respect to deposition processes. The higher values of the PM<sub>2.5</sub>/PM<sub>10</sub> ratio are observed over south-eastern Europe, Turkey, Ethiopia, and western parts of the Arabian Peninsula that are farther from the main dust sources.

Figure 10d shows the sum of surface concentrations of black carbon and organic matter  $(OC_1 + OC_2) * OC_{mfac} + BC_1 + BC_2$ . Their max, min, and mean concentration values are 31.8, 0.2, and 1.3 µg/m<sup>3</sup> respectively. Their contribution to aerosol pollution over the Arabian Peninsula in WRF-Chem simulations is fairly insignificant. Figure 10e shows the surface concentration of sea salt calculated as a sum of concentrations in each bin  $SEAS_2 + SEAS_3 + SEAS_4$ . Over the seas and coastal areas, the average concentration of sea salt is 3-12 µg/m<sup>3</sup>. In summer, strong winds in *Somali jet* (see Fig. 3b intensify sea salt



emission over the Arabian Sea, creating high surface concentrations of sea salt ( $27\text{--}42\text{ }\mu\text{g}/\text{m}^3$ ) along the coasts of Somalia and Oman. Due to prevailing northern winds, the transport of sea salt from the Mediterranean Sea to Egypt and Libya is observed.

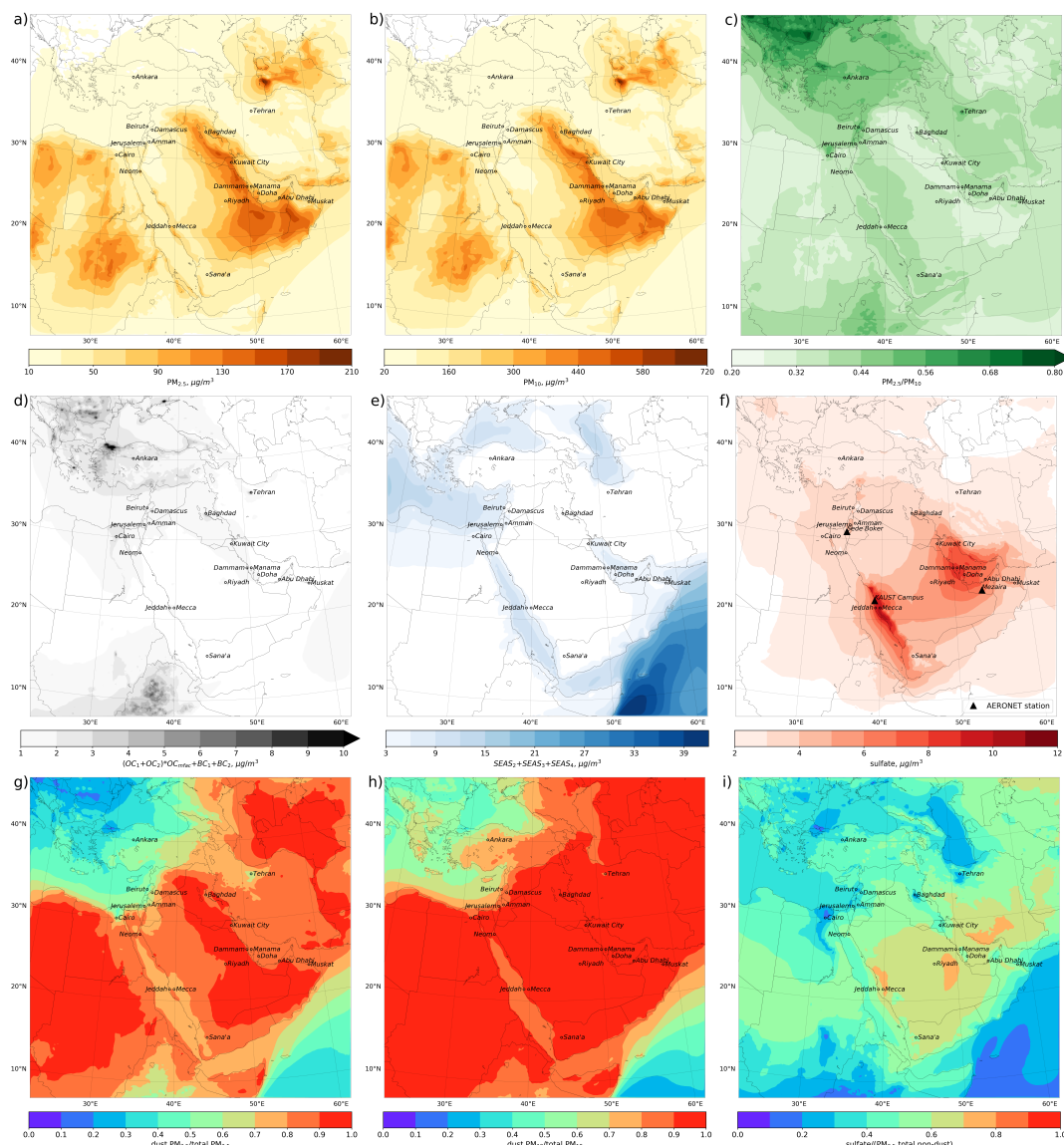


**Figure 10.** WRF-Chem's average 2015-2016 surface concentrations, ( $\mu\text{g}/\text{m}^3$ ): a)  $\text{PM}_{2.5}$ , b)  $\text{PM}_{10}$ ; c) ratio  $\text{PM}_{2.5}/\text{PM}_{10}$ ; d) black carbon and organic matter ( $((\text{OC}_1 + \text{OC}_2) * \text{OC}_{\text{mfac}} + \text{BC}_1 + \text{BC}_2)$ , ( $\mu\text{g}/\text{m}^3$ ), e) sea salt ( $\text{SEAS}_2 + \text{SEAS}_3 + \text{SEAS}_4$ ), ( $\mu\text{g}/\text{m}^3$ ), f) sulfate, ( $\mu\text{g}/\text{m}^3$ ) and locations of AERONET stations, g) ratio dust  $\text{PM}_{2.5}/(\text{total PM}_{2.5})$ , h) ratio dust  $\text{PM}_{10}/(\text{total PM}_{10})$ , i) ratio sulfate/ $(\text{PM}_{2.5}$  total non-dust). Abbreviations of the aerosols' names correspond to those given in Sec. 5.3.



510 The relatively high sulfate surface concentration (see Fig. 10f) is observed in the vicinity of the strong  $SO_2$  sources located along the west and east coast of Saudi Arabia and over the Arabian Gulf, as well as downwind from those sources. Figure 10f also denotes the locations of the AERONET stations, as in Fig. 1. The sulfate concentration at the *KAUST Campus* site is higher than at the *Mezaira* and *Sede Boker* AERONET sites (see Sec. 5.2.1) so it experiences more pronounced contribution of sulfate particulates into the fine mode of the AVSD (see Fig. 4a and Fig. 5).

515 Due to the prevailing northern winds along the Red Sea, sulfate aerosols originating from  $SO_2$  emissions along the Red Sea coast spread along the west coast of the Arabian Peninsula towards Yemen. The drift of sulfate from the Arabian Gulf into the interior of the Eastern part of the Arabian Peninsula is also seen. The sulfate annual mean background surface concentration over the US for the period 2003–2012, obtained in Buchard et al. (2016), is  $2\text{--}3\text{ }\mu\text{g}/\text{m}^3$ , similar to the background concentrations we see in the ME. But in the downwind or in the vicinity of strong  $SO_2$  point emissions, sulfate concentrations are 3–4 times  
 520 higher. Similar sulfate surface concentrations for the period 2000–2016 over the US were obtained in van Donkelaar et al. (2019), where the concentrations reach  $\approx 10\text{ }\mu\text{g}/\text{m}^3$  over the eastern part of the US during summer. In Al-Taani et al. (2019) the average 1980–2016 sulfate concentration computed for UAE is 2.5–3 times lower. This difference is caused by the fact that in Al-Taani et al. (2019), sulfate fields were taken from MERRA-2 reanalysis, which underestimates the  $SO_2$  emissions.

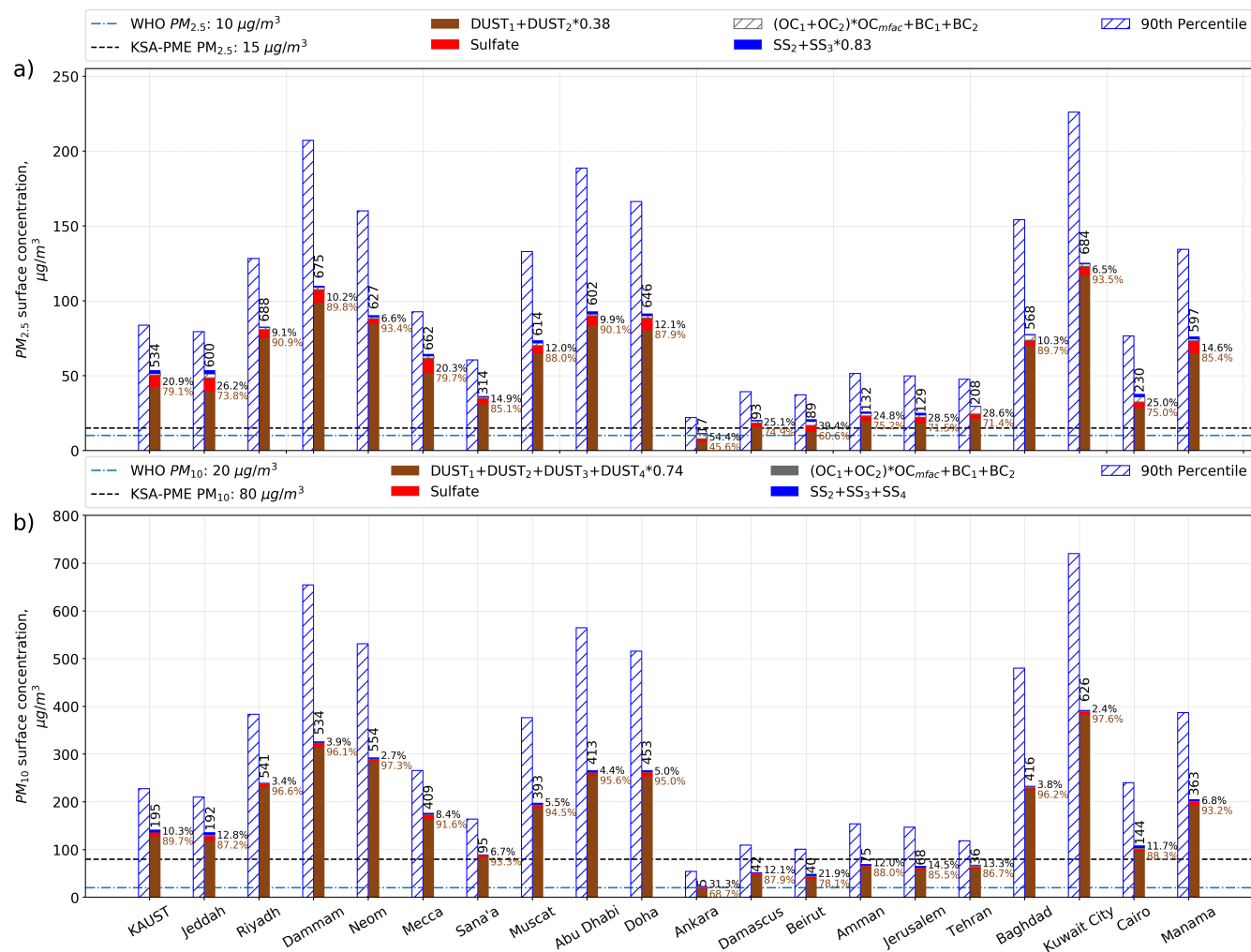
Contributions of dust to  $PM_{2.5}$  and  $PM_{10}$  calculated as ratios of dust  $PM_{2.5}$  to total  $PM_{2.5}$ , and dust  $PM_{10}$  to total  $PM_{10}$ ,  
 525 are shown in Fig. 10g and 10h respectively. Due to relatively low dust surface concentrations over the eastern Mediterranean, Turkey, and south-eastern Europe, the contribution of dust to  $PM_{2.5}$  and  $PM_{10}$  is 20–50% and 50–80%, respectively. In other areas that are closer to the dust source regions, the contribution of dust to PM is above 90%.

Figure 10i shows the ratio between the concentration of sulfate aerosol with respect to the total concentration of  $PM_{2.5}$  non-dust aerosols. The max, min, and mean values of this ratio are 0.76, 0.07, and 0.45, respectively. This ratio is low over the  
 530 seas where sea salt is prevalent but consistently exceeds 0.6 over land. Sulfate, therefore, is the primary anthropogenic pollutant over land. In the Arabian Coastal areas, central and southern parts of Saudi Arabia, and over south Iran, sulfate contributes 60–80% to the total  $PM_{2.5}$  non-dust aerosols concentration. Over the other parts of the Arabian Peninsula, the northern part of Sudan, Libya, and Egypt, sulfate contributes approximately 40–60% to total  $PM_{2.5}$  non-dust aerosols concentration.

### 5.3.4 Air-pollution in urban centers

535 To evaluate the air-quality in the ME's major cities, we calculate for their locations the average 2015–2016 daily  $PM_{2.5}$  and  $PM_{10}$  surface concentrations, their 90th percentiles, and we also calculate the contribution of the dust and non-dust components into PM (see Fig. 11). We calculate the number of days during the 2015–2016 period when the daily  $PM_{2.5}$  and  $PM_{10}$  surface concentrations exceed the US-EPA air-quality limit of  $35\text{ }\mu\text{g}/\text{m}^3$  and  $150\text{ }\mu\text{g}/\text{m}^3$  respectively.

Figure 11 shows that the annually-averaged  $PM_{10}$  and  $PM_{2.5}$  exceed the WHO air-quality guidelines 2–20 and 2–12 times,  
 540 respectively in all major cities of the ME, except Ankara. The KSA-PME air-quality limit for annual mean  $PM_{10}$  is exceeded by up to 5 times, and by up to 8 times for  $PM_{2.5}$ . Due to the lack of strong dust sources nearby, air-quality conditions in the cities in the eastern Mediterranean are more favorable when compared with those in the Arabian Peninsula. In these cities, the air-pollution shifts from natural to anthropogenic, as the contribution of non-dust aerosols to  $PM_{2.5}$  increases up to 40%, in



**Figure 11.** Annual mean 2015-2016 PM surface concentrations ( $\mu\text{g}/\text{m}^3$ ) calculated for the ME major cities and PM decomposition into dust and non-dust (sulfate, sea salt, black carbon and organic matter) components (stacked bars). Abbreviations of the aerosols' names correspond to those given in Sec. 5.3. Hatched bars denote 90th percentiles ( $\mu\text{g}/\text{m}^3$ ) calculated using daily mean PM concentrations. WHO guidelines and KSA-PME air-quality limits for annual averaged PM are shown by dash-dotted and dashed lines. Numbers over the stacked bars correspond to the number of days during 2015-2016, when daily averaged PM surface concentration exceeded US-EPA air-quality limit: a) PM<sub>2.5</sub>. Daily averaged US-EPA air-quality limit is  $35 \mu\text{g}/\text{m}^3$ . Annual WHO guideline and KSA-PME limit are  $10$  and  $15 \mu\text{g}/\text{m}^3$ , respectively; b) PM<sub>10</sub>. Daily averaged US-EPA air-quality limit is  $150 \mu\text{g}/\text{m}^3$ . Annual WHO and KSA-PME limits are  $20$  and  $80 \mu\text{g}/\text{m}^3$ , respectively.

contrast with the cities located in the Arabian Peninsula, where this contribution is up to 6-26%. Sulfate aerosol is the major contributor to non-dust PM<sub>2.5</sub>.



The cities at the eastern coast of the Arabian Peninsula and Baghdad have the highest 90th percentiles of daily mean PM concentrations. For example, in Dammam, Abu Dhabi, Doha, Kuwait City, and Baghdad, the 90th percentiles of daily mean surface concentration of  $PM_{10}$  and  $PM_{2.5}$  exceed 500-750 and 150-230  $\mu\text{g}/\text{m}^3$  respectively. This is above the KSA-PME air-quality limits for daily mean  $PM_{10}$  and  $PM_{2.5}$ .

550 In the Eastern Mediterranean cities, within the 2015-2016 period, the US-EPA air-quality daily mean limits are exceeded 5-75 days for  $PM_{10}$  and 7-208 days for  $PM_{2.5}$ . In the cities of the Arabian Peninsula, Iraq, and Iran, the US-EPA PM daily mean limits are exceeded 95-626 days for  $PM_{10}$  and 230-684 days for  $PM_{2.5}$  during the same period.

## 6 Conclusions

This study presents, for the first time, an evaluation of the advanced components of aerosol data assimilation products, MERRA-2 and CAMS-OA, over the Middle East. For this purpose, we collected the unique  $PM_{2.5}$  and  $PM_{10}$  measurements  
 555 taken in the biggest Saudi Arabian cities, retrievals of aerosol size distribution, and advanced satellite products. For the first time, we compared the new MODIS AOD retrieval, MAIAC, with the conventional MODIS-DB&DT AOD over the dust source regions of the Middle East. In the scope of this study, we conducted advanced two-year high-resolution WRF-Chem simulations. The WRF-Chem code was corrected to better describe the aerosol effects, and a new capability of using MERRA-2  
 560 output for boundary and initial conditions has been developed. To improve the calculation of sulfate aerosols, the most accurate  $SO_2$  emission dataset retrieved from OMI observations using the “top-down” approach was implemented in WRF-Chem. The contribution of natural dust, sea salt, and anthropogenic aerosols into the PM was estimated. We found that the three-bin approximation in CAMS-OA is not enough to correctly represent the aerosol size distribution, and MERRA-2 overestimates sea salt and underestimates sulfate concentrations. The air pollution in the major Middle Eastern cities is evaluated.

565 We evaluate the PM air-pollution over the ME during the 2015-2016 period using the regional WRF-Chem model v3.7.1, MERRA-2 and CAMS-OA assimilation products, and satellite and ground-based AOD observations, as well as *in situ*  $PM_{2.5}$  and  $PM_{10}$  surface concentration measurements available for 2016.

The regional WRF-Chem model has an advantage of higher spatial resolution ( $10\text{ km} \times 10\text{ km}$ ) versus global MERRA-2 ( $0.625^\circ \times 0.5^\circ$ ) and CAMS-OA ( $0.8^\circ \times 0.8^\circ$  before 21 June 2016, and  $0.4^\circ \times 0.4^\circ$  thereafter). We have modified the WRF-Chem  
 570 code to correct the discovered model deficiencies. These bug fixes have been implemented in the official WRF-Chem v4.1.3 release. The dust emission and its size distribution are tuned to fit the observed AOD and AVSD. To consistently account for the trans-boundary pollutant transport, MERRA-2 reanalysis was used to construct initial and boundary conditions for WRF-Chem both for meteorological fields and chemistry species. For this, we developed the new pre-processing utility named *Merra2BC* available at (<http://github.com/saneku/Merra2BC>). We equipped WRF-Chem with the novel OMI-HTAP  $SO_2$  emission data-  
 575 set (Liu et al., 2018) based on the combination of  $SO_2$  emissions taken from the HTAP-2.2 inventory with the catalogue of strong  $SO_2$  point emission sources (Fioletov et al., 2016). This allows us to improve calculation of sulfate aerosol and its contribution to PM.



The model and assimilation products struggle to fit the retrieved AERONET AVSD, failing to correctly reproduce the fine mode in the sub-micron range. MERRA-2 and WRF-Chem use the GOCART aerosol model with the same five dustbins and demonstrate a better agreement with the AERONET AVSD than CAMS-OA that uses only three dustbins. CAMS-OA overestimates the volume of fine dust particles with radii of 0.55-0.9  $\mu\text{m}$  and underestimates the volume of coarse dust particles with radii of 0.9-20  $\mu\text{m}$  in comparison with AERONET's AVSD. This CAMS-OA deficiency has been corrected with the latest system upgrade in 2019 by the introduction of a new desert dust scheme (Nabat et al., 2012). AOD and aerosol concentrations are linked through aerosol size distribution and optical properties.

We use in this study AOD observed by three AERONET stations and AOD from two MODIS retrieval products: MODIS-DB&DT and MAIAC. The AOD observations reflect the effect of the mixture of all aerosols, but over the ME land areas dust is dominant. The MODIS-DB&DT and MAIAC retrievals are not identical and the differences between them, with the most accurate AERONET AOD, advise the level of intrinsic AOD retrieval uncertainty. At all AERONET sites, WRF-Chem, CAMS-OA, MERRA-2, MODIS-DB&DT, and MAIAC reproduce quite well the magnitude and temporal evolution of the AERONET AOD time series during the whole considered period. MERRA-2 and MAIAC have the highest correlation with respect to AERONET AOD. CAMS-OA shows better correlation than MODIS-DB&DT, although CAMS-OA overestimates AERONET AOD, especially during the severe dust events and exhibits the relatively high positive *BIAS*. The MODIS-DB&DT and MAIAC retrieval products have similar absolute values of the mean *BIAS*, which is slightly larger than that of MERRA-2 and WRF-Chem. The MODIS-DB&DT AOD is biased positively except at *KAUST Campus* in 2016, but the MAIAC AOD is biased negatively except for *Sede Boker* for both years.

The model fields and assimilation products exhibit similar AOD seasonal patterns. CAMS-OA overestimates MODIS-DB&DT AOD during spring and summer but has the best agreement with MODIS-DB&DT during the autumn and winter. During summer, WRF-Chem shows higher AOD over the south-eastern part of the Arabian Peninsula in comparison with MODIS-DB&DT AOD. In general, MERRA-2 underestimates the MODIS-DB&DT AOD during summer. During winter and fall, WRF-Chem and MERRA-2 AODs are close, but both of them slightly underestimate the MODIS-DB&DT AOD. The AOD fields from MERRA-2 and CAMS-OA have the highest spatial correlation and lowest *RMSE* with respect to MODIS-DB&DT AOD. MAIAC underestimates AOD over the whole domain during all seasons in comparison with MODIS-DB&DT.

MODON AQMS observations of daily mean  $\text{PM}_{2.5}$  concentrations at all locations never drop below the WHO limit of 25  $\mu\text{g}/\text{m}^3$ . The less restrictive KSA-PME limit of 35  $\mu\text{g}/\text{m}^3$  is exceeded by 7-11 times. The daily mean  $\text{PM}_{10}$  MODON measurements exceed the WHO guideline of 50  $\mu\text{g}/\text{m}^3$  at all locations.  $\text{PM}_{10}$  concentration is higher in Riyadh and especially in Dammam in comparison with Jeddah. In Dammam the KSA-PME limit for daily averaged  $\text{PM}_{10}$  of 340  $\mu\text{g}/\text{m}^3$  is more frequently exceeded than in Jeddah, especially during the summer period. Annually averaged MODON measurements are 8-11 times higher than the WHO guideline of 20  $\mu\text{g}/\text{m}^3$  and 2-3 times higher than the KSA-PME limit of 80  $\mu\text{g}/\text{m}^3$ .

The capability of WRF-Chem, MERRA-2, and CAMS-OA in reproducing the ME air-quality is tested against AQMS measurements. In Jeddah and Riyadh WRF-Chem and MERRA-2 are able to reproduce the  $\text{PM}_{10}$  measurements quite well, but both of them overestimate observations in Dammam. CAMS-OA underestimates the  $\text{PM}_{10}$  surface concentrations in the ME region primarily due to deficiency in the dust size distribution.  $\text{PM}_{10}$  concentrations from CAMS-OA are 1.5-3.0 times smaller





in comparison with those from MERRA-2 and WRF-Chem. In Riyadh and Jeddah WRF-Chem, and MERRA-2 underestimate  $PM_{2.5}$  in comparison with MODON observations during 2016 about twice. However, both WRF-Chem and MERRA-2  $PM_{2.5}$  concentrations are in relatively good agreement with MODON observations in Dammam. CAMS-OA  $PM_{2.5}$  concentrations are higher than in WRF-Chem and MERRA-2 capturing  $PM_{2.5}$  observations better than other products in Jeddah and Riyadh.

We use WRF-Chem output to conduct the PM composition analysis. We found that the annual average  $PM_{2.5}/PM_{10}$  ratio over the ME is 0.38. It decreases to 0.2-0.3 over the major dust source regions, i.e. along the eastern Arabian peninsula, Iraq, and northern Africa. In most parts of the ME, dust is the major contributor to PM, but in the eastern Mediterranean and Turkey contribution of the dust component to  $PM_{2.5}$  and  $PM_{10}$  decreases to 20-50% and 50-80%, respectively.

Sulfate aerosol contributes to  $PM_{2.5}$  in the areas where strong  $SO_2$  sources are present, i.e., in the west and east coasts of Saudi Arabia and over the Arabian Gulf. In these areas sulfate surface concentration reaches  $8-11 \mu g/m^3$ , while the "clean" background level is  $2-4 \mu g/m^3$ . High sulfate content along the west coast of Saudi Arabia is consistent with the increased volume of the fine mode in the KAUST Campus AERONET AVSD in comparison with AVSDs from other sites. Sulfate is the major non-dust pollutant over the ME. Sulfate aerosols contribute 60-80 % to the total  $PM_{2.5}$  non-dust aerosols over the western and eastern Arabian coasts, over the central and southern parts of Saudi Arabia, and over the southern Iran. Over the other parts of Arabian Peninsula, northern Sudan, Libya, and Egypt, sulfate contributes approximately 40-60 % to the total  $PM_{2.5}$  non-dust aerosol concentration.

The analysis of the annually averaged  $PM_{2.5}$  and  $PM_{10}$  surface concentrations in the ME major cities conducted using WRF-Chem output shows a very high level of PM pollution. In Dammam, Abu Dhabi, Doha, Kuwait City, and Baghdad, the 90th percentile of  $PM_{10}$  and  $PM_{2.5}$  annual mean surface concentrations exceed  $500-750$  and  $150-230 \mu g/m^3$  respectively, which is above the KSA-PME air-quality limit. In the eastern Mediterranean, dust concentration drops, and the contribution of non-dust aerosols to  $PM_{2.5}$  increases up to 25-40%. In the cities located in the Arabian Peninsula contribution of the non-dust component to  $PM_{2.5}$  is 6-26%, which limits the emission control on air-quality. In the eastern Mediterranean cities during the 2015-2016 period, the daily mean surface PM concentrations exceed the US-EPA air quality daily mean limit 5-75 days for  $PM_{10}$  and 7-208 days for  $PM_{2.5}$ . In the ME cities over the Arabian peninsula, Iraq, and Iran, the US-EPA air-quality daily mean limit is exceeded 95-626 days for  $PM_{10}$  and 230-684 days for  $PM_{2.5}$ .

In Jeddah and Dammam, WRF-Chem and MERRA-2 show similar contributions of the non-dust component to  $PM_{2.5}$  (25-33% in Jeddah and 10-14% in Dammam). In MERRA-2, however, sea salt is a major non-dust contributor to  $PM_{2.5}$ , while in WRF-Chem it is sulfate. In CAMS-OA contribution of the non-dust particulates to  $PM_{2.5}$  in Jeddah and Dammam is  $\approx 7-11\%$ . In Riyadh, the contribution of the non-dust component to  $PM_{2.5}$  is  $\approx 9-11\%$  for both MERRA-2 and WRF-Chem.

In Jeddah, Riyadh, and Dammam, the contribution of black carbon to  $PM_{2.5}$  and  $PM_{10}$  is not significant in WRF-Chem and both assimilation products. In MERRA-2, the contribution of organic matter to  $PM_{2.5}$  is more substantial in comparison with WRF-Chem and CAMS-OA. However, in CAMS-OA,  $PM_{10}$  has more organic matter than in WRF-Chem and MERRA-2. We also observe the relative increase of organic matter in  $PM_{2.5}$  (except WRF-Chem in some cases) and  $PM_{10}$  in Jeddah and Dammam in comparison with Riyadh.





Thus, in this study, we found that MERRA-2 and CAMS-OA assimilation products, as well as WRF-Chem output despite some intrinsic uncertainties, could be successfully used for evaluation the air-quality over the Arabian Peninsula. All products show the dominant contribution of mineral dust into PM. However, in the Arabian coastal areas where  $SO_2$  emissions are high, both contributions of sulfate and sea salt could be significant. The developed WRF-Chem modeling framework can be used to simulate other pollutants like  $NO_2$  and  $O_3$ . The results of the current research could serve as the basis for an improved air-quality forecast system that interactively calculates high-resolution radiative, dynamical, atmospheric chemistry and aerosol processes, driven by natural and anthropogenic emissions. This system will be especially valuable for the prediction of extreme pollution events. It will also improve understanding of the impact of anthropogenic and natural pollution on air quality and human health in the ME region.

#### *Code availability.*

1. *Merra2BC* interpolation utility is available at <http://github.com/saneku/Merra2BC>

#### *Data availability.*

1. MERRA-2 is available at <https://disc.gsfc.nasa.gov/daac-bin/FTPSubset2.pl>
2. CAMS-OA is available at <http://apps.ecmwf.int/datasets/data/cams-nrealtime>
3. MODIS-DB&DT AOD data are available at <https://giovanni.gsfc.nasa.gov>
4. AERONET data are available at <https://aeronet.gsfc.nasa.gov/>
5. MAIAC data are available at <https://lpdaac.usgs.gov/products/mcd19a2v006/>
6. HTAP-2.2 is available at [http://edgar.jrc.ec.europa.eu/htap\\_v2/index.php?SECURE=123](http://edgar.jrc.ec.europa.eu/htap_v2/index.php?SECURE=123)

## **Appendix A**

### **A1 Merra2BC interpolation utility**

*Merra2BC* interpolator (available at <https://github.com/saneku/Merra2BC>) creates time-varying chemical boundary conditions based on MERRA-2 reanalysis for a WRF-Chem simulation by interpolating chemical species mixing ratios defined on the MERRA-2 grid to the WRF-Chem grid for initial conditions and boundary conditions. In the case of initial conditions, interpolated values are written to each node of the WRF-Chem grid. In the case of boundary conditions, only boundary nodes are affected.

*Merra2BC* utility is written in Python. The utility requires additional modules which need to be installed in the Python environment: NetCDF4 interface (to work with netCDF files) and SciPy's interpolation package.



The full MERRA-2 reanalysis dataset including aerosol fields is publicly available online (see "Code and data availability" section). Depending on the requirements, one or both of the following aerosol and gaseous collections need to be downloaded: *inst3\_3d\_aer\_Nv* - gaseous and aerosol mixing ratios (kg/kg) and *inst3\_3d\_chm\_Nv* - Carbon monoxide and Ozone mixing ratios (kg/kg). In addition to downloaded mixing ratios, pressure thickness DELP and surface pressure PS fields also need to be downloaded. Spatial coverage of the MERRA-2 files should include the area of the WRF-Chem simulation domain. The time span of the downloaded files should match with the start and duration of the WRF-Chem simulation. For more information regarding MERRA-2 files specification please refer to Bosilovich et al. (2016).

### A1.1 Mapping chemical species between MERRA-2 and WRF-Chem

The *Merra2BC* input file *config.py* contains multiplication factors to convert MERRA-2 mixing ratios of gases given in kg/kg to ppmv. Aerosols are converted from kg/kg to µg/kg. When using the GOCART aerosol module in the WRF-Chem simulation, all MERRA-2 aerosols and gases are matched with those from WRF-Chem. To convert MERRA-2 aerosol mixing ratios given in kg/kg into µg/kg, multiply by a factor of  $10^9$ . In the case of gases, multiply MERRA-2 mixing ratios by a ratio of molar masses  $M_{air}/M_{gas}$  multiplied by  $10^6$  to convert kg/kg to ppmv, where  $M_{gas}$  and  $M_{air}$  are the corresponding molar masses. If another aerosol module is chosen in WRF-Chem, then different multiplication factors should be used.

### A1.2 Typical workflow

Below are the steps describing how to work with the *Merra2BC* utility:

1. Run *real.exe*, which will produce the initial *wrfinput\_d01* and boundary conditions *wrfbdy\_d01* files required by WRF-Chem simulation
2. Download required MERRA-2 collection files
3. Download the *Merra2BC* code from <https://github.com/saneku/Merra2BC>
4. Edit *config.py* file which contains:
  - (a) Mapping of chemical species and aerosols between MERRA-2 and WRF-Chem
  - (b) Paths to *wrfinput\_d01*, *wrfbdy\_d01*, *met\_em...\** files;
  - (c) Path to the downloaded MERRA-2 collection files
5. Program *real.exe* sets default boundary and initial conditions for some chemical species. *Merra2BC* adds interpolated values to the existing ones and it may cause incorrect concentration values. To avoid this, run script "*zero\_fields.py*", which will zero the required fields
6. Run script "*main.py*", which will perform the interpolation; as a result, files *wrfinput\_d01*, *wrfbdy\_d01* will be updated by the values interpolated from MERRA-2
7. Modify WRF-Chem *namelist.input* file at section *&chem*: set *have\_bcs\_chem* = *.true.* to activate updated boundary conditions from MERRA-2 and, if it is needed, *chem\_in\_opt* = 1 to activate updated initial conditions;
8. Run *wrf.exe* program.



For the usage of the *Merra2BC* interpolator the following python modules need to be installed:

- netcdf4: <https://github.com/Unidata/netcdf4-python>
- scipy: <https://github.com/scipy/scipy>

### A1.3 Meteorological Boundary and Initial Conditions

To be consistent with BC&IC for chemical species and aerosols, we utilized the same procedure to build meteorological BC&IC from MERRA-2 reanalysis for all required meteorological parameters. In particular, the following 3D parameters were processed: pressure (Pa), geopotential height (m), temperature (K), meridional and zonal wind components (m/s), relative humidity (%); 2D parameters: surface pressure (Pa), sea level pressure (Pa), meridional and zonal wind components at 10m (m/s), temperature at 2m (K), relative humidity at 2m (%), skin temperature (K), ice mask (0/1), terrain height (m), land/sea mask (1/0), soil temperature at 0-10 (cm), 10-40 (cm), 40-100 (cm) and 100-200 (cm); soil moisture at 0-10 (cm), 10-40 (cm), 40-100 (cm) and 100-200 (cm); snow depth (m); snow water equivalent (kg/m<sup>2</sup>).

### A2 Statistics

We calculated the following statistical parameters to quantify the level of agreement between estimations and observations:

Pearson correlation coefficient ( $R$ ):

$$R = \frac{\sum_{i=1}^N (F_i - \bar{F})(O_i - \bar{O})}{\sqrt{\sum_{i=1}^N (F_i - \bar{F})^2 \sum_{i=1}^N (O_i - \bar{O})^2}}. \quad (\text{A1})$$

Root mean square error ( $RMSE$ ):

$$RMSE = \sqrt{\frac{1}{N} \sum_{i=1}^N (F_i - O_i)^2} \quad (\text{A2})$$

Mean bias ( $BIAS$ ):

$$BIAS = \frac{1}{N} \sum_{i=1}^N (F_i - O_i) \quad (\text{A3})$$

where  $F_i$  is the estimated value,  $O_i$  is the observed value,  $\bar{F} = \frac{1}{N} \sum_{i=1}^N F_i$  and  $\bar{O} = \frac{1}{N} \sum_{i=1}^N O_i$  their averages and  $N$  is the number of data.

*Author contributions.* A. Ukhov wrote the manuscript and constructed IC&BC for aerosol and chemistry species based on MERRA-2 reanalysis, and took part in planning and performing the calculations. S. Mostamandi performed the calculations, constructed meteorological



730 BC&IC based on MERRA-2 reanalysis, prepared MAIAC AOD fields, wrote the section on meteorological conditions, and took part in the discussions. G. Stenchikov planned the calculations, led the discussion, and reviewed and improved the manuscript. I. Shevchenko maintained the *KAUST Campus* AERONET station. Y. Alshehri collected, filtered, and validated PM observational data and wrote the section on the PM measurement procedures. J. Flemming and A. Dasilva participated in the discussion, helped to formulate the research program, and reviewed the manuscript.

*Competing interests.* The authors declare that they have no conflict of interest.

735 *Acknowledgements.* In this work we used AERONET data from the *KAUST Campus* site that was established and maintained by our group with the help of the NASA Goddard Space Flight Center AERONET team. We thank Brent Holben and Alexander Smirnov for the monitoring and regular calibrations of our instruments. We also used data from the *Sede Boker* and *Mezaira* sites and would like to thank their principal investigators Arnon Karnieli and Brent Holben.

740 The research reported in this publication was supported by funding from King Abdullah University of Science and Technology (KAUST). For computer time, this research used the resources of the Supercomputing Laboratory at KAUST. The authors would like to thank the Saudi Authority for Industrial Cities and Technology Zones (MODON) for sharing their air quality observational data.

We are thankful to Linda and Mark Everett for proofreading this manuscript.



## References

- Acker, J. G. and Leptoukh, G.: Online analysis enhances use of NASA earth science data, *Eos, Transactions American Geophysical Union*, 88, 14–17, 2007.
- Al-Jeelani, H. A.: Air quality assessment at Al-Taneem area in the Holy Makkah City, Saudi Arabia, *Environmental monitoring and assessment*, 156, 211, 2009.
- Al-Taani, A. A., Nazzal, Y., Howari, F. M., and Yousef, A.: Long-term trends in ambient fine particulate matter from 1980 to 2016 in United Arab Emirates, *Environmental monitoring and assessment*, 191, 143, 2019.
- Alghamdi, M. A., Almazroui, M., Shamy, M., Redal, M. A., Alkhalaf, A. K., Hussein, M. A., and Khoder, M. I.: Characterization and elemental composition of atmospheric aerosol loads during springtime dust storm in western Saudi Arabia, *Aerosol Air Qual. Res.*, 15, 440–453, 2015.
- Anderson, J. R.: A land use and land cover classification system for use with remote sensor data, vol. 964, US Government Printing Office, 1976.
- Anisimov, A., Tao, W., Stenchikov, G., Kalenderski, S., Prakash, P. J., Yang, Z.-L., and Shi, M.: Quantifying local-scale dust emission from the Arabian Red Sea coastal plain, *Atmos. Chem. Phys.*, 17, 993–1015, 2017.
- Anisimov, A., Axisa, D., Kucera, P. A., Mostamandi, S., and Stenchikov, G.: Observations and Cloud-Resolving Modeling of Haboob Dust Storms Over the Arabian Peninsula, *Journal of Geophysical Research: Atmospheres*, 123, 12–147, 2018.
- Archer-Nicholls, S., Lowe, D., Darbyshire, E., Morgan, W., Bela, M., Pereira, G., Trembath, J., Kaiser, J., Longo, K., Freitas, S., et al.: Characterising Brazilian biomass burning emissions using WRF-Chem with MOSAIC sectional aerosol, *Geoscientific Model Development*, 8, 549–577, 2015.
- Bangalath, H. K. and Stenchikov, G.: Sensitivity of the Middle East–North African Tropical Rainbelt to Dust Shortwave Absorption: A High-Resolution AGCM Experiment, *Journal of Climate*, 29, 7103–7126, 2016.
- Banks, J. R., Brindley, H. E., Stenchikov, G., and Schepanski, K.: Satellite retrievals of dust aerosol over the Red Sea and the Persian Gulf (2005–2015), *Atmospheric Chemistry and Physics*, 17, 3987–4003, 2017.
- Benedetti, A., Morcrette, J.-J., Boucher, O., Dethof, A., Engelen, R., Fisher, M., Flentje, H., Huneeus, N., Jones, L., Kaiser, J., et al.: Aerosol analysis and forecast in the European centre for medium-range weather forecasts integrated forecast system: 2. Data assimilation, *Journal of Geophysical Research: Atmospheres*, 114, 2009.
- Bosilovich, M., Lucchesi, R., and Suarez, M.: MERRA-2: File specification GMAO Office Note No. 9 (Version 1.1), 2016.
- Brindley, H., Osipov, S., Bantges, R., Smirnov, A., Banks, J., Levy, R., Jish Prakash, P., and Stenchikov, G.: An assessment of the quality of aerosol retrievals over the Red Sea and evaluation of the climatological cloud-free dust direct radiative effect in the region, *Journal of Geophysical Research: Atmospheres*, 120, 10–862, 2015.
- Buchard, V., da Silva, A., Randles, C., Colarco, P., Ferrare, R., Hair, J., Hostetler, C., Tackett, J., and Winker, D.: Evaluation of the surface PM<sub>2.5</sub> in Version 1 of the NASA MERRA Aerosol Reanalysis over the United States, *Atmospheric Environment*, 125, 100–111, 2016.
- Buchard, V., Randles, C., Da Silva, A., Darmenov, A., Colarco, P., Govindaraju, R., Ferrare, R., Hair, J., Beyersdorf, A., Ziemba, L., et al.: The MERRA-2 aerosol reanalysis, 1980 onward. Part II: Evaluation and case studies, *Journal of Climate*, 30, 6851–6872, 2017.
- Cahill, B., Toumi, R., Stenchikov, G., Osipov, S., and Brindley, H.: Evaluation of thermal and dynamic impacts of summer dust aerosols on the Red Sea, *Journal of Geophysical Research: Oceans*, 122, 1325–1346, 2017.
- Carlson, T. N. and Benjamin, S. G.: Radiative heating rates for Saharan dust, *Journal of the Atmospheric Sciences*, 37, 193–213, 1980.



- 780 Cesnulyte, V., Lindfors, A., Pitkänen, M., Lehtinen, K., Morcrette, J.-J., and Arola, A.: Comparing ECMWF AOD with AERONET observations at visible and UV wavelengths, *Atmospheric Chemistry and Physics*, 14, 593–608, 2014.
- Charlson, R. J., Schwartz, S., Hales, J., Cess, R. D., Coakley, J. J., Hansen, J., and Hofmann, D.: Climate forcing by anthropogenic aerosols, *Science*, 255, 423–430, 1992.
- Chin, M., Ginoux, P., Kinne, S., Torres, O., Holben, B. N., Duncan, B. N., Martin, R. V., Logan, J. A., Higurashi, A., and Nakajima, T.:  
 785 Tropospheric aerosol optical thickness from the GOCART model and comparisons with satellite and Sun photometer measurements, *Journal of the atmospheric sciences*, 59, 461–483, 2002.
- Chuang, C. C., Penner, J. E., Taylor, K. E., Grossman, A. S., and Walton, J. J.: An assessment of the radiative effects of anthropogenic sulfate, *Journal of Geophysical Research: Atmospheres*, 102, 3761–3778, 1997.
- Chuang, M.-T., Zhang, Y., and Kang, D.: Application of WRF/Chem-MADRID for real-time air quality forecasting over the Southeastern  
 790 United States, *Atmospheric Environment*, 45, 6241–6250, 2011.
- Climate.com: Climate of Middle East, Climate.com, <http://climateof.com/middleeast/index.asp>, 2018.
- Cuevas, E., Camino, C., Benedetti, A., Basart, S., Terradellas, E., Baldasano, J., Morcrette, J.-J., Marticorena, B., Goloub, P., Mortier, A., et al.: The MACC-II 2007–2008 reanalysis: atmospheric dust evaluation and characterization over Northern Africa and Middle East., *Atmospheric Chemistry & Physics Discussions*, 14, 2014.
- 795 Damian, V., Sandu, A., Damian, M., Potra, F., and Carmichael, G. R.: The kinetic preprocessor KPP-a software environment for solving chemical kinetics, *Computers & Chemical Engineering*, 26, 1567–1579, 2002.
- Dubovik, O. and King, M. D.: A flexible inversion algorithm for retrieval of aerosol optical properties from Sun and sky radiance measurements, *Journal of Geophysical Research: Atmospheres*, 105, 20 673–20 696, 2000.
- EUEA: Air Quality Standards, European Environment Agency, <http://ec.europa.eu/environment/air/quality/standards.htm>, 2008.
- 800 Farahat, A.: Air pollution in the Arabian Peninsula (Saudi Arabia, the United Arab Emirates, Kuwait, Qatar, Bahrain, and Oman): causes, effects, and aerosol categorization, *Arabian Journal of Geosciences*, 9, 196, 2016.
- Fioletov, V. E., McLinden, C. A., Krotkov, N., Li, C., Joiner, J., Theys, N., Carn, S., and Moran, M. D.: A global catalogue of large SO<sub>2</sub> sources and emissions derived from the Ozone Monitoring Instrument., *Atmospheric Chemistry & Physics*, 16, 2016.
- Flemming, J., Huijnen, V., Arteta, J., Bechtold, P., Beljaars, A., Blechschmidt, A.-M., Diamantakis, M., Engelen, R., Gaudel, A., Inness, A.,  
 805 et al.: Tropospheric chemistry in the Integrated Forecasting System of ECMWF., *Geoscientific model development*, 8, 2015.
- Forkel, R., Werhahn, J., Hansen, A. B., McKeen, S., Peckham, S., Grell, G., and Suppan, P.: Effect of aerosol-radiation feedback on regional air quality—A case study with WRF/Chem, *Atmospheric environment*, 53, 202–211, 2012.
- Furman, H. K. H.: Dust storms in the Middle East: sources of origin and their temporal characteristics, *Indoor and Built Environment*, 12, 419–426, 2003.
- 810 Ginoux, P., Chin, M., Tegen, I., Prospero, J. M., Holben, B., Dubovik, O., and Lin, S.-J.: Sources and distributions of dust aerosols simulated with the GOCART model, *Journal of Geophysical Research: Atmospheres*, 106, 20 255–20 273, 2001.
- Gong, S.: A parameterization of sea-salt aerosol source function for sub-and super-micron particles, *Global biogeochemical cycles*, 17, 2003.
- Goudie, A. S. and Middleton, N. J.: *Desert dust in the global system*, Springer Science & Business Media, 2006.
- Granier, C., Bessagnet, B., Bond, T., D’Angiola, A., van Der Gon, H. D., Frost, G. J., Heil, A., Kaiser, J. W., Kinne, S., Klimont, Z., et al.:  
 815 Evolution of anthropogenic and biomass burning emissions of air pollutants at global and regional scales during the 1980–2010 period, *Climatic Change*, 109, 163, 2011.





- Grell, G. A., Peckham, S. E., Schmitz, R., McKeen, S. A., Frost, G., Skamarock, W. C., and Eder, B.: Fully coupled “online” chemistry within the WRF model, *Atmospheric Environment*, 39, 6957–6975, 2005.
- Hamidi, M., Kavianpour, M. R., and Shao, Y.: Synoptic analysis of dust storms in the Middle East, *Asia-Pacific Journal of Atmospheric Sciences*, 49, 279–286, 2013.
- Heidinger, A. K., Foster, M. J., Walther, A., and Zhao, X.: The pathfinder atmospheres–extended AVHRR climate dataset, *Bulletin of the American Meteorological Society*, 95, 909–922, 2014.
- Holben, B. N., Eck, T. F., Slutsker, I., Tanre, D., Buis, J., Setzer, A., Vermote, E., Reagan, J., Kaufman, Y., Nakajima, T., et al.: AERONET—A federated instrument network and data archive for aerosol characterization, *Remote sensing of environment*, 66, 1–16, 1998.
- Hsu, N. C., Tsay, S.-C., King, M. D., and Herman, J. R.: Deep blue retrievals of Asian aerosol properties during ACE-Asia, *IEEE Transactions on Geoscience and Remote Sensing*, 44, 3180–3195, 2006.
- Inness, A., Blechschmidt, A.-M., Bouarar, I., Chabrilat, S., Crepulja, M., Engelen, R., Eskes, H., Flemming, J., Gaudel, A., Hendrick, F., et al.: Data assimilation of satellite-retrieved ozone, carbon monoxide and nitrogen dioxide with ECMWF’s Composition-IFS, *Atmospheric chemistry and physics*, 15, 5275–5303, 2015.
- Janssens-Maenhout, G., Pagliari, V., Guizzardi, D., and Muntean, M.: Global emission inventories in the Emission Database for Global Atmospheric Research (EDGAR)—Manual (I), Gridding: EDGAR emissions distribution on global gridmaps, Publications Office of the European Union, Luxembourg, 2013.
- Janssens-Maenhout, G., Crippa, M., Guizzardi, D., Dentener, F., Muntean, M., Pouliot, G., Keating, T., Zhang, Q., Kurokawa, J., Wankmüller, R., et al.: HTAP\_v2: a mosaic of regional and global emission gridmaps for 2008 and 2010 to study hemispheric transport of air pollution., *Atmospheric Chemistry & Physics Discussions*, 15, 2015.
- Jish Prakash, P., Stenchikov, G. L., Kalenderski, S., Osipov, S., and Bangalath, H. K.: The impact of dust storms on the Arabian Peninsula and the Red Sea, *Atmospheric Chemistry and Physics*, 2015.
- Jish Prakash, P., Stenchikov, G., Tao, W., Yapici, T., Warsama, B., and Engelbrecht, J. P.: Arabian Red Sea coastal soils as potential mineral dust sources, *Atmospheric Chemistry and Physics*, 16, 11 991–12 004, 2016.
- Kahn, R. A., Gaitley, B. J., Martonchik, J. V., Diner, D. J., Crean, K. A., and Holben, B.: Multiangle Imaging Spectroradiometer (MISR) global aerosol optical depth validation based on 2 years of coincident Aerosol Robotic Network (AERONET) observations, *Journal of Geophysical Research: Atmospheres*, 110, 2005.
- Kalenderski, S. and Stenchikov, G.: High-resolution regional modeling of summertime transport and impact of African dust over the Red Sea and Arabian Peninsula, *Journal of Geophysical Research: Atmospheres*, 121, 6435–6458, 2016.
- Kalenderski, S., Stenchikov, G. L., and Zhao, C.: Modeling a typical winter-time dust event over the Arabian Peninsula and the Red Sea, *Atmospheric Chemistry and Physics*, 2013.
- Karagulian, F., Belis, C. A., Dora, C. F. C., Prüss-Ustün, A. M., Bonjour, S., Adair-Rohani, H., and Amann, M.: Contributions to cities’ ambient particulate matter (PM): A systematic review of local source contributions at global level, *Atmospheric environment*, 120, 475–483, 2015.
- Karagulian, F., Temimi, M., Ghebreyesus, D., Weston, M., Kondapalli, N. K., Valappil, V. K., Aldababesh, A., Lyapustin, A., Chaouch, N., Al Hammadi, F., et al.: Analysis of a severe dust storm and its impact on air quality conditions using WRF-Chem modeling, satellite imagery, and ground observations, *Air Quality, Atmosphere & Health*, pp. 1–18, 2019.
- Kaufman, Y. J., Tanré, D., Remer, L. A., Vermote, E., Chu, A., and Holben, B.: Operational remote sensing of tropospheric aerosol over land from EOS moderate resolution imaging spectroradiometer, *Journal of Geophysical Research: Atmospheres*, 102, 17 051–17 067, 1997.



- 855 Khan, B., Stenchikov, G., Weinzierl, B., Kalenderski, S., and Osipov, S.: Dust plume formation in the free troposphere and aerosol size distribution during the Saharan Mineral Dust Experiment in North Africa, *Tellus B: Chemical and Physical Meteorology*, 67, 27 170, 2015.
- Khodeir, M., Shamy, M., Alghamdi, M., Zhong, M., Sun, H., Costa, M., Chen, L.-C., and Maciejczyk, P.: Source apportionment and elemental composition of PM<sub>2.5</sub> and PM<sub>10</sub> in Jeddah City, Saudi Arabia, *Atmospheric pollution research*, 3, 331–340, 2012.
- 860 Kim, S.-W., Heckel, A., McKeen, S., Frost, G., Hsie, E.-Y., Trainer, M., Richter, A., Burrows, J., Peckham, S., and Grell, G.: Satellite-observed US power plant NO<sub>x</sub> emission reductions and their impact on air quality, *Geophysical Research Letters*, 33, 2006.
- Klingmüller, K., Pozzer, A., Metzger, S., Stenchikov, G. L., and Lelieveld, J.: Aerosol optical depth trend over the Middle East, *Atmospheric Chemistry and Physics*, 16, 5063–5073, 2016.
- Kok, J. F.: Does the size distribution of mineral dust aerosols depend on the wind speed at emission?, *Atmospheric Chemistry and Physics*, 11, 10 149–10 156, 2011.
- 865 Lelieveld, J., Evans, J. S., Fnais, M., Giannadaki, D., and Pozzer, A.: The contribution of outdoor air pollution sources to premature mortality on a global scale, *Nature*, 525, 367, 2015.
- Levelt, P. F., van den Oord, G. H., Dobber, M. R., Malkki, A., Visser, H., de Vries, J., Stammes, P., Lundell, J. O., and Saari, H.: The ozone monitoring instrument, *IEEE Transactions on geoscience and remote sensing*, 44, 1093–1101, 2006.
- 870 Li, C., Joiner, J., Krotkov, N. A., and Bhartia, P. K.: A fast and sensitive new satellite SO<sub>2</sub> retrieval algorithm based on principal component analysis: Application to the ozone monitoring instrument, *Geophysical Research Letters*, 40, 6314–6318, 2013.
- Lihavainen, H., Alghamdi, M., Hyvärinen, A.-P., Hussein, T., Aaltonen, V., Abdelmaksoud, A., Al-Jeelani, H., Almazroui, M., Almeahmadi, F., Al Zawad, F., et al.: Aerosols physical properties at Hada Al Sham, western Saudi Arabia, *Atmospheric Environment*, 135, 109–117, 2016.
- 875 Liu, F., Choi, S., Li, C., Fioletov, V. E., McLinden, C. A., Joiner, J., Krotkov, N. A., Bian, H., Janssens-Maenhout, G., Darmenov, A. S., et al.: A new global anthropogenic SO<sub>2</sub> emission inventory for the last decade: a mosaic of satellite-derived and bottom-up emissions, *Atmospheric Chemistry and Physics*, 18, 16 571–16 586, 2018.
- Lyapustin, A., Wang, Y., Korkin, S., and Huang, D.: MODIS Collection 6 MAIAC algorithm., *Atmospheric Measurement Techniques*, 11, 2018.
- 880 Madronich, S.: Photodissociation in the atmosphere: 1. Actinic flux and the effects of ground reflections and clouds, *Journal of Geophysical Research: Atmospheres*, 92, 9740–9752, 1987.
- Marticorena, B. and Bergametti, G.: Modeling the atmospheric dust cycle: 1. Design of a soil-derived dust emission scheme, *Journal of Geophysical Research: Atmospheres*, 100, 16 415–16 430, 1995.
- McLinden, C. A., Fioletov, V., Shephard, M. W., Krotkov, N., Li, C., Martin, R. V., Moran, M. D., and Joiner, J.: Space-based detection of missing sulfur dioxide sources of global air pollution, *Nature Geoscience*, 9, 496–500, 2016.
- 885 Middleton, N.: A geography of dust storms in South-west Asia, *Journal of Climatology*, 6, 183–196, 1986.
- Miguez-Macho, G., Stenchikov, G. L., and Robock, A.: Spectral nudging to eliminate the effects of domain position and geometry in regional climate model simulations, *Journal of Geophysical Research: Atmospheres*, 109, 2004.
- Miller, R. and Tegen, I.: Climate response to soil dust aerosols, *Journal of climate*, 11, 3247–3267, 1998.
- 890 Mohalfi, S., Bedi, H., Krishnamurti, T., and Cocke, S. D.: Impact of shortwave radiative effects of dust aerosols on the summer season heat low over Saudi Arabia, *Monthly weather review*, 126, 3153–3168, 1998.



- Morcrette, J.-J., Boucher, O., Jones, L., Salmond, D., Bechtold, P., Beljaars, A., Benedetti, A., Bonet, A., Kaiser, J., Razinger, M., et al.: Aerosol analysis and forecast in the European Centre for medium-range weather forecasts integrated forecast system: Forward modeling, *Journal of Geophysical Research: Atmospheres*, 114, 2009.
- 895 Munir, S., Habeebullah, T. M., Seroji, A. R., Morsy, E. A., Mohammed, A. M., Saud, W. A., Abdou, A. E., and Awad, A. H.: Modeling particulate matter concentrations in Makkah, applying a statistical modeling approach, *Aerosol Air Qual. Res.*, 13, 901–910, 2013.
- Myhre, G., Shindell, D., Bréon, F., Collins, W., Fuglestad, J., Huang, J., Koch, D., Lamarque, J., Lee, D., Mendoza, B., et al.: Climate change 2013: the physical science basis. Contribution of Working Group I to the Fifth Assessment Report of the Intergovernmental Panel on Climate Change, K., Tignor, M., Allen, S.K., Boschung, J., Nauels, A., Xia, Y., Bex, V., and Midgley, P.M., Cambridge University Press  
 900 Cambridge, United Kingdom and New York, NY, USA, 2013.
- Nabat, P., Solmon, F., Mallet, M., Kok, J., and Somot, S.: Dust emission size distribution impact on aerosol budget and radiative forcing over the Mediterranean region: a regional climate model approach., *Atmospheric Chemistry & Physics Discussions*, 12, 2012.
- Nayebare, S. R., Aburizaiza, O. S., Khwaja, H. A., Siddique, A., Hussain, M. M., Zeb, J., Khatib, F., Carpenter, D. O., and Blake, D. R.: Chemical characterization and source apportionment of PM<sub>2.5</sub> in Rabigh, Saudi Arabia, *Aerosol and Air Quality Research*, 16, 3114–  
 905 3129, 2016.
- Notaro, M., Alkolibi, F., Fadda, E., and Bakhrjy, F.: Trajectory analysis of Saudi Arabian dust storms, *Journal of Geophysical Research: Atmospheres*, 118, 6028–6043, 2013.
- Notaro, M., Yu, Y., and Kalashnikova, O. V.: Regime shift in Arabian dust activity, triggered by persistent Fertile Crescent drought, *Journal of Geophysical Research: Atmospheres*, 120, 2015.
- 910 Osipov, S. and Stenchikov, G.: Simulating the regional impact of dust on the Middle East climate and the Red Sea, *Journal of Geophysical Research: Oceans*, 123, 1032–1047, 2018.
- Osipov, S., Stenchikov, G., Brindley, H., and Banks, J.: Diurnal cycle of the dust instantaneous direct radiative forcing over the Arabian Peninsula, *Atmospheric Chemistry and Physics*, 15, 9537–9553, 2015.
- Parajuli, S. P., Stenchikov, G. L., Ukhov, A., and Kim, H.: Dust emission modeling using a new high-resolution dust source function in  
 915 WRF-Chem with implications for air quality, *Journal of Geophysical Research: Atmospheres*, 2019.
- PME: Ambient Air Quality Standard, The Presidency of Meteorology and Environment, 2012.
- Prospero, J. M., Ginoux, P., Torres, O., Nicholson, S. E., and Gill, T. E.: Environmental characterization of global sources of atmospheric soil dust identified with the Nimbus 7 Total Ozone Mapping Spectrometer (TOMS) absorbing aerosol product, *Reviews of geophysics*, 40, 2–1, 2002.
- 920 Provençal, S., Buchard, V., da Silva, A. M., Leduc, R., and Barrette, N.: Evaluation of PM surface concentrations simulated by Version 1 of NASA's MERRA Aerosol Reanalysis over Europe, *Atmospheric pollution research*, 8, 374–382, 2017.
- Ramanathan, V., Chung, C., Kim, D., Bettge, T., Buja, L., Kiehl, J., Washington, W., Fu, Q., Sikka, D., and Wild, M.: Atmospheric brown clouds: Impacts on South Asian climate and hydrological cycle, *Proceedings of the National Academy of Sciences*, 102, 5326–5333, 2005.
- Randles, C., da Silva, A. M., Buchard, V., Colarco, P., Darmenov, A., Govindaraju, R., Smirnov, A., Holben, B., Ferrare, R., Hair, J., et al.:  
 925 The MERRA-2 aerosol reanalysis, 1980 onward. Part I: System description and data assimilation evaluation, *Journal of climate*, 30, 6823–6850, 2017.
- Reid, J. S., Piketh, S. J., Walker, A. L., Burger, R. P., Ross, K. E., Westphal, D. L., Bruintjes, R. T., Holben, B. N., Hsu, C., Jensen, T. L., et al.: An overview of UAE2 flight operations: Observations of summertime atmospheric thermodynamic and aerosol profiles of the southern Arabian Gulf, *Journal of Geophysical Research: Atmospheres*, 113, 2008.



- 930 Rienecker, M. M., Suarez, M., Todling, R., Bacmeister, J., Takacs, L., Liu, H., Gu, W., Sienkiewicz, M., Koster, R., Gelaro, R., et al.: The  
 GEOS-5 Data Assimilation System: Documentation of Versions 5.0. 1, 5.1. 0, and 5.2. 0, Tech. rep., NASA Goddard Space Flight Center,  
 Greenbelt, Maryland, 2008.
- Ritter, M., Müller, M. D., Tsai, M.-Y., and Parlow, E.: Air pollution modeling over very complex terrain: an evaluation of WRF-Chem over  
 Switzerland for two 1-year periods, *Atmospheric research*, 132, 209–222, 2013.
- 935 Shao, Y.: A model for mineral dust emission, *Journal of Geophysical Research: Atmospheres*, 106, 20 239–20 254, 2001.
- Shao, Y.: *Physics and modelling of wind erosion*, vol. 37, Springer Science & Business Media, 2008.
- Shi, Y., Zhang, J., Reid, J., Holben, B., Hyer, E., and Curtis, C.: An analysis of the collection 5 MODIS over-ocean aerosol optical depth  
 product for its implication in aerosol assimilation, *Atmospheric Chemistry and Physics*, 11, 557–565, 2011.
- Skamarock, W. C., Klemp, J. B., Dudhia, J., Gill, D. O., Barker, D. M., Wang, W., and Powers, J. G.: A description of the advanced research  
 940 WRF version 2, Tech. rep., National Center For Atmospheric Research Boulder Co Mesoscale and Microscale Meteorology Div, 2005.
- Stockwell, W. R., Kirchner, F., Kuhn, M., and Seefeld, S.: A new mechanism for regional atmospheric chemistry modeling, *Journal of  
 Geophysical Research: Atmospheres*, 102, 25 847–25 879, 1997.
- Tawabini, B. S., Lawal, T. T., Shaibani, A., and Farahat, A. M.: Morphological and Chemical Properties of Particulate Matter in the Dammam  
 Metropolitan Region: Dhahran, Khobar, and Dammam, Saudi Arabia, *Advances in Meteorology*, 2017, 2017.
- 945 USEPA: National Ambient Air Quality Standards, USEPA, <https://www.epa.gov/criteria-air-pollutants/naaqs-table>, 2010.
- van Donkelaar, A., Martin, R. V., Li, C., and Burnett, R. T.: Regional Estimates of Chemical Composition of Fine Particulate Matter using a  
 Combined Geoscience-Statistical Method with Information from Satellites, Models, and Monitors, *Environmental science & technology*,  
 2019.
- Wang, X., Liang, X.-Z., Jiang, W., Tao, Z., Wang, J. X., Liu, H., Han, Z., Liu, S., Zhang, Y., Grell, G. A., et al.: WRF-Chem simulation of  
 950 East Asian air quality: Sensitivity to temporal and vertical emissions distributions, *Atmospheric Environment*, 44, 660–669, 2010.
- WHO: Air quality guidelines: global update 2005, WHO, 2006.
- WHO: Ambient air quality and health, WHO, [http://www.who.int/en/news-room/fact-sheets/detail/ambient-\(outdoor\)  
 -air-quality-and-health](http://www.who.int/en/news-room/fact-sheets/detail/ambient-(outdoor)-air-quality-and-health), 2018.
- Yarwood, G., Rao, S., Yocke, M., and Whitten, G.: Updates to the carbon bond chemical mechanism: CB05, Final report to the US EPA,  
 955 RT-0400675, 8, 2005.
- Yu, Y., Notaro, M., Liu, Z., Wang, F., Alkolibi, F., Fadda, E., and Bakhryy, F.: Climatic controls on the interannual to decadal variability in  
 Saudi Arabian dust activity: Toward the development of a seasonal dust prediction model, *Journal of Geophysical Research: Atmospheres*,  
 120, 1739–1758, 2015.
- Yu, Y., Notaro, M., Kalashnikova, O. V., and Garay, M. J.: Climatology of summer Shamal wind in the Middle East, *Journal of Geophysical  
 960 Research: Atmospheres*, 121, 289–305, 2016.
- Zender, C. S., Miller, R., and Tegen, I.: Quantifying mineral dust mass budgets: Terminology, constraints, and current estimates, *Eos, Trans-  
 actions American Geophysical Union*, 85, 509–512, 2004.